ENG. Struct. Civ. Eng. 2026, 20(4): 757–780
https://doi.org/10.1007/s11709-026-1303-y

RESEARCH ARTICLE

Influence of polyethylene fiber and rebar type on shear performance of engineered cementitious composites beams mixed with seawater and sea sand

Zheming WEN[a], Qinghai XIE[a,b*], Jie ZENG[a], Songling XUE[a,c], Chao MA[a]

[a] *School of Civil and Ocean Engineering, Jiangsu Ocean University, Lianyungang 222005, China*
[b] *Department of Structural Engineering, Tongji University, Shanghai 200092, China*
[c] *School of Civil Engineering, Southwest Jiaotong University, Chengdu 611756, China*
[*] *Corresponding author. E-mail: qinghai2019@jou.edu.cn*

ABSTRACT This study adopted natural seawater and sea sand, and 1%–2% and 12–24 mm polyethylene (PE) fibers to develop seawater and sea sand mixed engineered cementitious composites (SS-ECC). The shear performance of 17 SS-ECC beams without stirrups was then assessed, considering the influence of PE fibers and rebar types. Results showed that increasing the PE fiber content significantly enhanced the tensile strength and flexural toughness of SS-ECC. As the fiber content increased from 1% to 1.5% and 2%, the tensile strength rose by 15.3% and 28.2%, respectively. The fiber length of 24 mm proved optimal, inducing tensile strength gains of 41.1% and 44.2% over lengths of 12 and 18 mm. While PE fibers showed limited impact on the shear capacity of steel-fiber-reinforced polymer (FRP) composite bar (SFCB) reinforced SS-ECC beams, they substantially enhanced the shear ductility. The use of low-modulus glass FRP and SFCB rebars reduced the shear capacity, particularly at a higher reinforcement ratio. This study finally proposes a unified shear capacity model for stirrup-free SS-ECC beams, which showed a favorable agreement with existing data. Results from this paper can help to advance the sustainable utilization of sea sand and seawater, and the shear design of SS-ECC components.

KEYWORDS PE fiber, seawater and sea sand, ECC, SFCB, shear performance

1 Introduction

With the rapid development of the modern construction industry, resources such as cement, water, and sand are being consumed rapidly [1–3]. To alleviate the shortage of water and sand resources for construction in coastal areas, scholars have begun to study seawater and sea sand mixed concrete [4–10]. Because this kind of concrete contains excess chloride ions, ordinary steel bars would easily corrode and pose a threat to structural safety. Therefore, fiber-reinforced polymer (FRP) bars of excellent corrosion resistance are generally adopted to replace steel bars, such as glass FRP (GFRP) and basalt FRP (BFRP) [3,11–13]. However, compared with steel bars, the relatively low elastic modulus of FRP bars would reduce the load-bearing capacity and ductility of the concrete components [14–16].

To address this issue, some researchers have combined FRP and steel bars to develop the steel-FRP composite bar (SFCB) with a high elastic modulus and deformation ability [17–19]. While the outer FRP wrap of the SFCB rebar provides favorable corrosion resistance, the steel core can enhance the whole modulus and ductility of the SFCB rebar [18,20]. Compared with the steel rebar, the SFCB rebar can provide both stable post-yield tensile modulus and tensile strength [21]. Studies revealed that concrete beams with SFCB rebars showed stable post-yield stiffness after the yielding of the inner steel bar [22]. Bai et al. [23] investigated the bond behavior of the SFCB and GFRP rebar in concrete and found that SFCB improved the bond strength under the same conditions. Test results by Ge et al. [24] showed that SFCB rebar

Article history: Received Jul 28, 2025; Accepted Jan 16, 2026

improved the bending stiffness and capacity of concrete beams compared with BFRP rebar reinforced components. Zhou et al. [25] adopted SFCB rebar to achieve a high displacement ductility factor from 3.7 to 4.9 for concrete beams under bending. Han et al. [26] proposed an equal stiffness design method for SFCB rebar reinforced concrete beams under bending. The above available experimental results concluded that the SFCB rebar can improve the bending capacity and ductility of concrete beams [25,26].

While studies have mainly focused on the bending behavior, the shear performance of SFCB rebar reinforced concrete components also draws some attention [27]. Yuan et al. [28] tested the shear behavior of concrete beams with both BFRP and SFCB rebar, and found that SFCB rebar increased the shear capacity by 8%–10%. The SFCB rebar also increased the deformation resistance and crack control capability. Han et al. [27] investigated the shear performance of SFCB and steel rebar reinforced beams without stirrups, and concluded that SFCB can improve the shear capacity of beams by 3.9%–40.3% due to the post-yielding stiffness. Due to the limited research on the shear performance of concrete components with SFCB rebars, the effect of SFCB rebars on shear capacity needs more investigation for proper shear design [28].

From the aspect of concrete, the utilization of engineered cementitious composites (ECC) provides an approach to improving the shear capacity and ductility of FRP reinforced concrete components [29]. Due to the fiber bridging effect, ECC showed improved tensile strength and cracking behavior [30]. Hence, this can enhance the tensile properties of concrete and then increase the shear resistance of concrete components. For the same purpose of addressing the shortage of river sand and freshwater, seawater and sea sand mixed ECC (SS-ECC) has been developed. Huang et al. [31] adopted polyethylene (PE) fibers to obtain high-strength SS-ECC with compressive strength > 130 MPa, tensile strength > 8 MPa, and tensile strain capacity of about 5%. Then they proposed a probabilistic model for the stochastic cracking assessment of SS-ECC [32]. To assess the contribution of SS-ECC to the shear capacity of beams, Liao et al. [33] studied the shear behavior of 11 SS-ECC beams reinforced with BFRP bars, and found that the shear capacity of SS-ECC beams without stirrups was higher than that of beams with a stirrup ratio of 0.67%. PE fibers provided over 70% contribution to the shear capacity of BFRP reinforced SS-ECC beams without stirrups. They further tested SS-ECC beams with various seawater salinities [34] and found that SS-ECC contributed 60%–70% shear capacity while mortar only provided 30%–40%. With proper design, ECC can change the failure mode from shear to flexural and significantly improve the capacity of concrete components with the same amount of FRP reinforcement but without stirrups [29].

The above discussion demonstrates that SFCB rebar can improve the shear performance of FRP rebar reinforced beams. Meanwhile, SS-ECC can alleviate the shortage of river sand and freshwater and can also improve the shear behavior of FRP rebar reinforced beams. However, limited studies have been conducted on the shear performance of SFCB rebar reinforced SS-ECC beams [28]. Additional experimental data are needed to better quantify the shear contribution of SFCB rebar and SS-ECC, to achieve a reasonable design before wide application.

To address this knowledge gap, this paper studies the shear performance of SFCB rebar reinforced SS-ECC beams, with emphasis on the shear capacity and ductility of reinforced SS-ECC components. The strength and toughness of SS-ECC materials were first investigated, considering the influence of PE fiber content and length. Afterward, 17 reinforced beams without stirrups were tested under shear to figure out the effects of PE fibers and rebar types on the shear capacity and ductility. Finally, a unified formula was proposed to predict the shear capacity of SS-ECC beams longitudinally with steel rebar, GFRP rebar, and SFCB. The results from this paper can provide a reference for developing SS-ECC considering the shear contribution. This study can also contribute to the shear design of SFCB rebar reinforced SS-ECC beams without stirrups, promoting the application of seawater and sea sand, and addressing the scarcity of river sand and freshwater for coastal construction.

2 Research significance

With excellent corrosion resistance, FRP rebar can significantly promote the use of seawater and sea sand to alleviate the shortage of water and sand resources for construction in coastal areas. However, the low elastic modulus of FRP bars can lead to reduced shear capacity and ductility of concrete beams. To address this issue, this study adopted ECC and SFCB rebar to enhance the shear performance of concrete beams without stirrups. This paper first examines the effects of PE fiber content and length on the mechanical properties of SS-ECC. Afterward, this paper analyzes the influence of fiber characteristics, reinforcement type, and reinforcement ratio on the shear capacity and ductility of SS-ECC beams. This research proves that with proper design, SFCB rebar reinforced SS-ECC beams can achieve a favorable balance between shear capacity and ductility. The findings contribute valuable insights into the development of SS-ECC, and the shear design of SFCB rebar reinforced SS-ECC beams without stirrups. Meanwhile, this approach not only enhances structural strength but also helps mitigate the scarcity of natural sand and freshwater resources for coastal construction.

3 Specimen preparation and test methods

3.1 Raw materials

To study the shear performance of reinforced SS-ECC beams, the following factors were considered: fiber content, fiber length, reinforcement type, and reinforcement ratio.

The raw materials of ECC in this experiment were: P.O. 42.5 cement, limestone powder, silica fume, blast furnace slag, sea sand and river sand (as shown in Figs. 1(a) and 1(b)), seawater and tap water, polycarboxylate superplasticizer, and PE fiber (as shown in Figs. 1(c)–1(e)). The parameters of PE fibers are given in Table 1.

The rebars were SFCB with diameters of 12(8), 16(8), and 16(10) mm, GFRP bars with diameters of 12 and 16 mm, and HRB 400 steel bars with diameters of 12 and 16 mm. The pictures of SFCB and GFRP bars are shown in Fig. 1(f).

3.2 Specimen preparation

There were eight ECC mix ratios in this test, as shown in Table 2. For each mix, several types of specimens were prepared for material property tests: 3 prism specimens of 100 mm × 100 mm × 300 mm and 3 cube specimens of 70.7 mm × 70.7 mm × 70.7 mm for compressive tests, 3 prism specimens of 40 mm × 40 mm × 160 mm for flexural tests, and 6 dog-bone specimens of 368 mm × 100 mm × 50 mm for tensile tests.

There were a total of 17 ECC beams of 100 mm × 100 mm × 515 mm for shear tests. The test variables of ECC beams are shown in Table 3. The rebar layout within beams is presented in Fig. 2, and the dimensions of the ECC beams are given in Fig. 3.

In the production of ECC, cement, limestone powder, silica fume, blast furnace slag, and sand were mixed for about 3 min. Afterward, water was added and stirred for about 5 min. Then the PE fiber was gradually added and stirred for about 8 min, so that the PE fiber could be evenly distributed in the matrix of ECC. After mixing, the ECC was poured into plastic molds and vibrated evenly. After one day of curing, specimens were removed from the molds and cured at room temperature for 28 d.

3.3 Test setup

For better evaluation of the performance of ECC beams, a series of tests were conducted to obtain the mechanical properties of ECC. These tests included uniaxial tensile tests, uniaxial compressive tests, and four-point bending tests of ECC.

The uniaxial tensile tests of ECC were carried out on

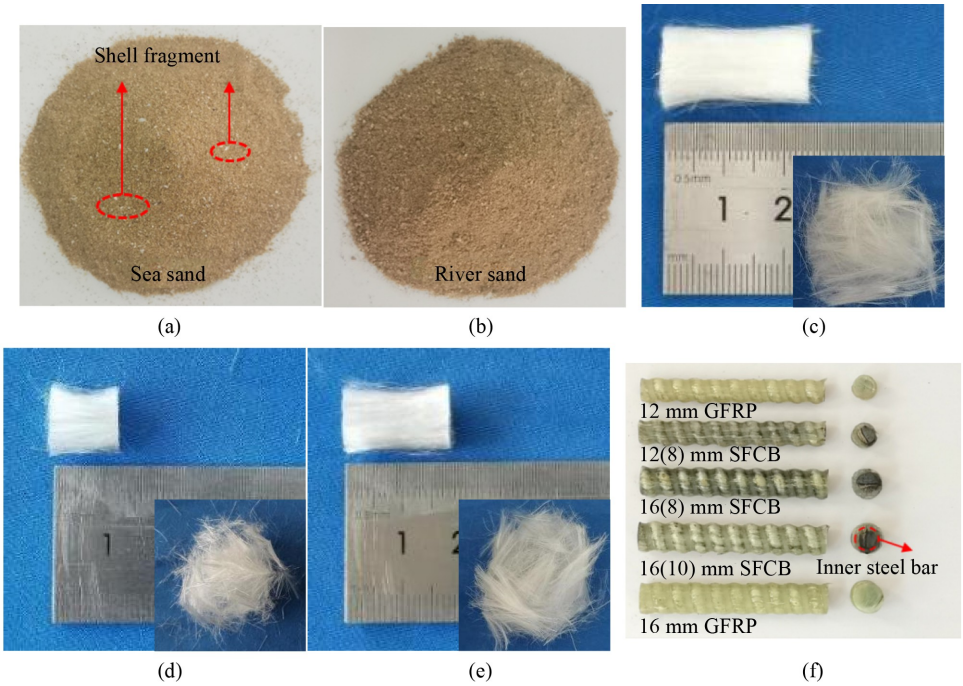

Fig. 1 Raw material: (a) sea sand; (b) river sand; (c) GFRP and SFCB bar; (d) 12 mm PE fiber; (e) 18 mm PE fiber; (f) 24 mm PE fiber.

Table 1 Physical properties of PE fiber

Length (mm)	Diameter (μm)	Density (g/cm^3)	Elastic modulus (GPa)	Tensile strength (MPa)	Ultimate tensile strain
12, 18, 24	25	0.97	⩾ 122	⩾ 3100	⩽ 3.5%

Table 2 Mix ratios of ECC

Mix identification	Cement	Limestone powder	Silica fume	Blast furnace slag	Sand	Water	Polycarboxylate superplasticizer	Fiber content (vol.%)	Fiber length (mm)
A-SSE	1	0.14	0.21	1.07	1.04 (sea sand)	0.6 (seawater)	0.015	1.0	12
B-SSE	1	0.14	0.21	1.07			0.015	1.5	12
C-SSE	1	0.14	0.21	1.07			0.015	2.0	12
D-SSE	1	0.14	0.21	1.07			0.015	1.5	18
E-SSE	1	0.14	0.21	1.07			0.015	1.5	24
N-SSM	1	0.14	0.21	1.07			0.015	0.0	0.0
B-ECC	1	0.14	0.21	1.07	1.04 (river sand)	0.6 (tap water)	0.015	1.5	12
N-MOR	1	0.14	0.21	1.07			0.015	0.0	0.0

Table 3 Design parameters of ECC beams

Number	Group name*	Rebar	Diameter (mm)	Rebar number
1	S12(8)-2-N-SSM	SFCB	12(8)	2
2	S12(8)-2-N-MOR	SFCB	12(8)	2
3	S12(8)-2-A-SSE	SFCB	12(8)	2
4	S12(8)-2-C-SSE	SFCB	12(8)	2
5	S12(8)-2-B-SSE	SFCB	12(8)	2
6	S12(8)-2-D-SSE	SFCB	12(8)	2
7	S12(8)-2-E-SSE	SFCB	12(8)	2
8	S12(8)-3-B-SSE	SFCB	12(8)	3
9	S16(8)-2-B-SSE	SFCB	16(8)	2
10	S16(10)-2-B-SSE	SFCB	16(10)	2
11	G12-2-B-SSE	GFRP	12	2
12	G16-2-B-SSE	GFRP	16	2
13	G12-3-B-SSE	GFRP	12	3
14	H12-2-B-SSE	HRB400	12	2
15	H16-2-B-SSE	HRB400	16	2
16	H12-3-B-SSE	HRB400	12	3
17	S12(8)-2-B-ECC	SFCB	12(8)	2

*Note: The group name consists of four parts. For example, S12(8)-2-N-SSM indicates the beam made of the N-SSM mix ratio in Table 2, reinforced with two 12(8) mm SFCB rebars.

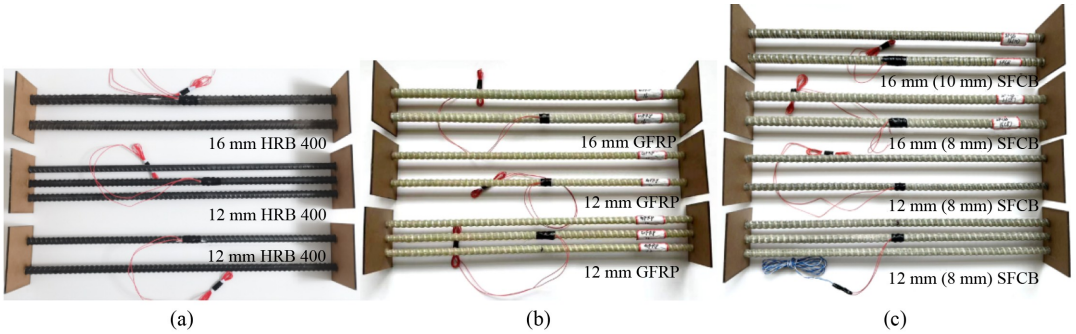

Fig. 2 Reinforcement arrangement in ECC beams: (a) HRB 400; (b) GFRP; (c) SFCB.

dog-bone specimens with a size of 368 mm × 100 mm × 50 mm. The sketch of the dog-bone specimen is shown in Fig. 4, according to the T/CCPA 7-2018 [35] standard.

The uniaxial compressive tests of ECC were conducted on a high-rigidity machine, as shown in Fig. 4. The whole compressive strain–stress curves were obtained, and the elastic modulus can be derived accordingly.

Four-point bending tests were carried out on ECC

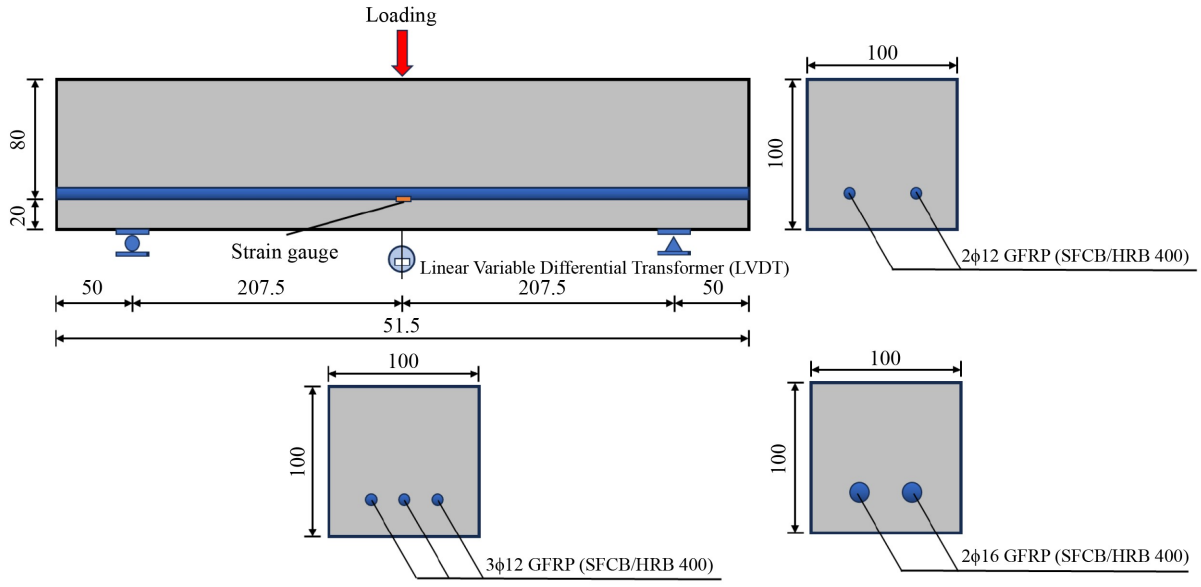

Fig. 3 Beam details and strain gauge layout (unit: mm).

specimens of 40 mm × 40 mm × 160 mm. The flexural deformation and crack development of the specimens were measured and analyzed by the DIC method (Fig. 4). The displacement control loading was adopted at the rate of 2 mm/min.

For shear tests of reinforced ECC beams, the three-point bending test method was adopted with a loading rate of 1 mm/min. Meanwhile, the DIC device was used to capture the cracking development of ECC beams. Before experiments, speckles were sprayed on the surface of the ECC beams, as shown in Fig. 4. During the test, the high-definition camera was set up to take photos every 2 s. After the test, DIC analysis software was used to process these photos [36]. LVDT was used to record the mid-span deflection of ECC specimens.

4 Test results and analysis of material properties of engineered cementitious composites

4.1 Axial tensile properties of engineered cementitious composites

The failure mode of the ECC under uniaxial tension is illustrated in Fig. 5. The incorporation of fibers significantly enhanced the ductility of the cementitious matrix, enabling ECC to develop multiple microcracks under tensile loading. Furthermore, the fibers contributed to a notable improvement in tensile strength, as summarized in Table 4**.** When fibers of varying dosages and lengths were introduced into the matrix, the resulting ECC exhibited a tensile strength approximately 2–3 times higher than that of plain mortar. Notably, the use of seawater and sea sand slightly improved the tensile strength of ECC. As the PE fiber content increased, the tensile strength of ECC demonstrated a consistent upward trend. These observations are in alignment with the findings proposed by Huang et al. [31]. The tensile strength of ECC peaked at the fiber length of 24 mm.

To assess fiber reinforcing effects quantitatively, this investigation employs Eqs. (1) and (2) for regression analysis.

$$f_t = f_{t0}(1 + \alpha\lambda), \tag{1}$$

$$\lambda = \rho_f \frac{L_f}{d_f}, \tag{2}$$

where f_t is the uniaxial tensile strength of ECC (MPa), f_{t0} is the uniaxial tensile strength of the matrix without fibers (MPa), α is the fiber influence coefficient, λ is fiber characteristic value, ρ_f is fiber volume content, l_f is fiber length (mm), d_f is fiber diameter (mm).

As shown in Fig. 6, the tensile strength of ECC demonstrated a positive correlation with fiber characteristic parameters. Linear fitting was then performed, which yielded an optimal value of α = 0.13716. A coefficient of determination (R^2) of 0.95 was obtained, as described in the aforementioned Refs. [37,38].

4.2 Axial compressive properties of engineered cementitious composites

4.2.1 Compressive strength of engineered cementitious composites

The compressive properties of ECC are summarized in Table 5 for all 8 groups of mix proportions. Table 5 shows that the compressive strength of ECC mixed with seawater and sea sand was higher than that of ECC mixed

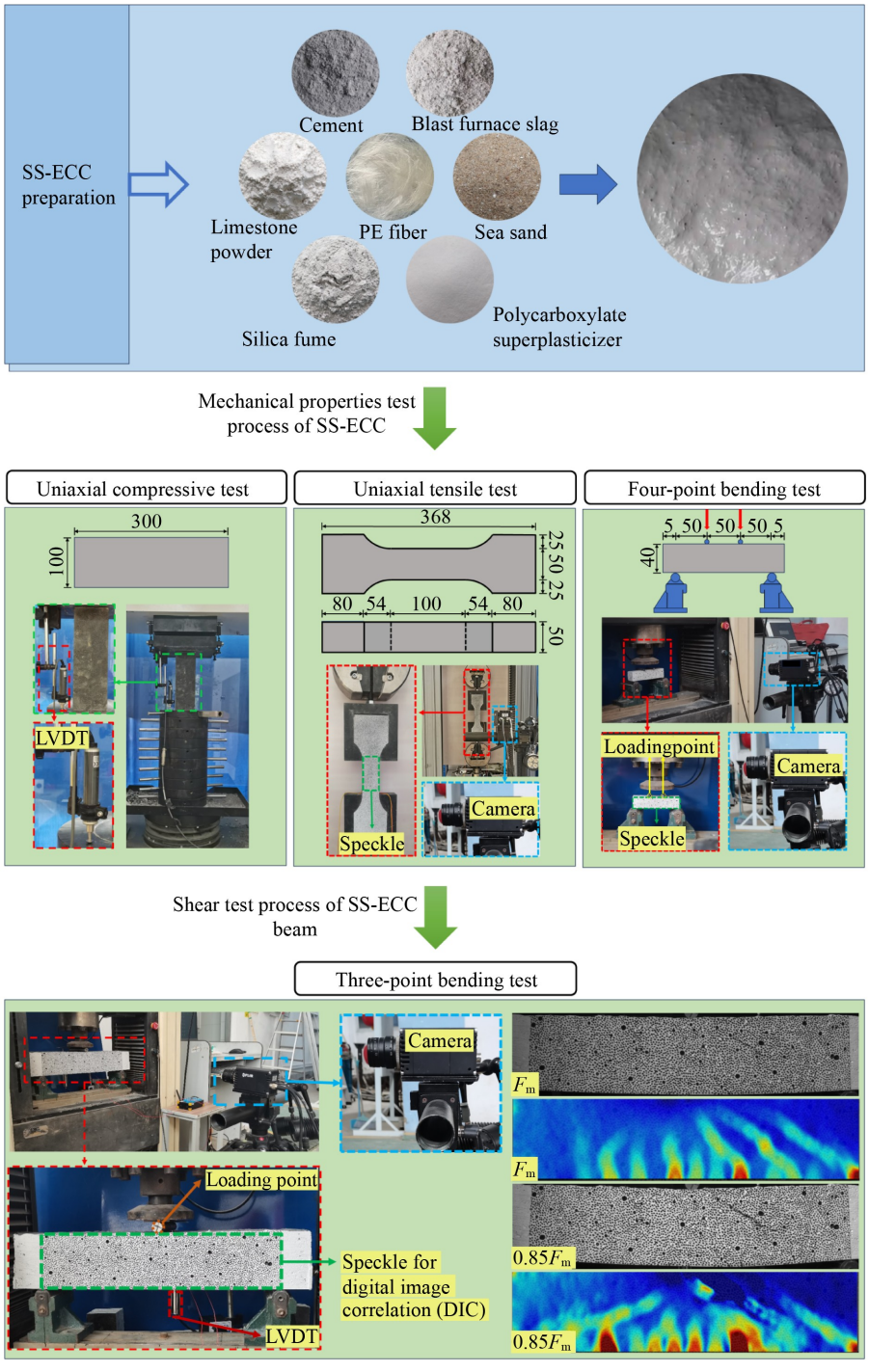

Fig. 4 Test procedures.

with tap water and river sand. This is mainly because the chloride ions in seawater and sea sand can accelerate the hydration of cement, and the resulting hydration product fills in the pores in ECC to densify the microstructure of ECC [39]. The compressive strength values of ECC show that the incorporation of PE fiber reduced the compressive strength of ECC. This observation is consistent with the research results of some scholars [31,40]. The decrease in compressive strength of ECC can be attributed to the micro-pores and micro-cracks induced by the presence of PE fibers.

Table 5 also shows that the ECC with 18 mm PE fiber showed the largest compressive strength at constant fiber content. The axial compressive strength of D-SSE was 6.6% and 16.1% higher than that of E-SSE and B-SSE, respectively. With the increase of PE fiber length from 12 to 24 mm, the axial compressive strength of ECC increased first and then decreased. Meanwhile, ECC

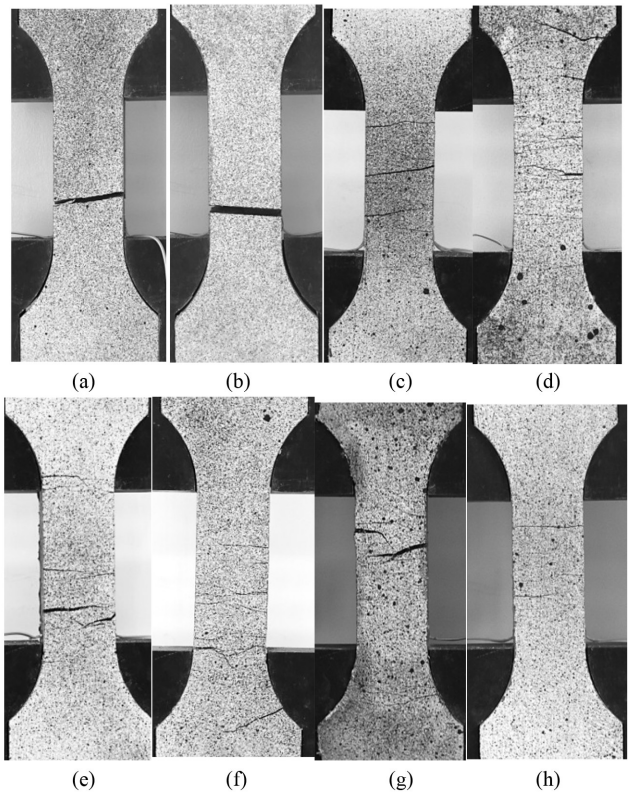

Fig. 5 Uniaxial tensile crack distribution of ECC: (a) MOR; (b) SSM; (c) 1%-12-SSE; (d) 1.5%-12-SSE; (e) 2%-12-SSE; (f) 1.5%-18-SSE; (g) 1.5%-24-SSE; (h) 1.5%-12-ECC.

Table 4 Tensile strength of ECC

Concrete type	Mixproportion	Tensile strength(MPa)	Standard deviation	Fiber characteristicvalue λ
1%-12-SSE	A-SSE	2.06	0.157	4.8
1.5%-12-SSE	B-SSE	2.29	0.140	7.2
1.5%-12-ECC	B-ECC	2.04	0.240	7.2
2%-12-SSE	C-SSE	2.64	0.273	9.6
1.5%-18-SSE	D-SSE	2.24	0.207	10.8
1.5%-24-SSE	E-SSE	3.23	0.340	14.4
MOR	N-MOR	0.97	0.046	–
SSM	N-SSM	1.08	0.177	–

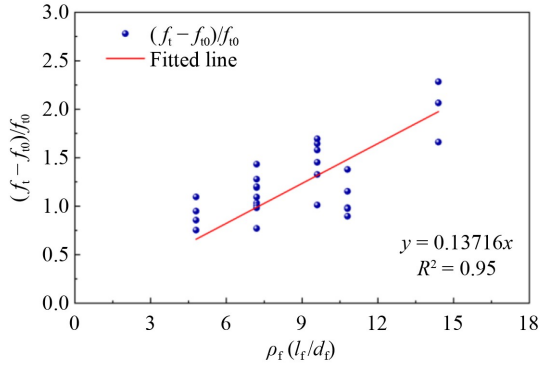

Fig. 6 Linear fitting of ECC tensile strength with fiber characteristic value.

containing 1% and 2% PE fiber demonstrated comparable compressive performance, measuring 19.87% and 18.78% higher, respectively, than those with 1.5% fiber content.

4.2.2 Elastic modulus

The test results of the elastic modulus of ECC are also shown in Table 5. The elastic modulus of ECC without PE fiber was higher than that of ECC with PE fiber. The elastic modulus of SSM and MOR was 22.78 and 17.44 GPa, respectively, which was 43.8% and 30.22% higher than that of SSE and ECC with 1.5% 12 mm PE fiber. The above data show that the incorporation of PE fiber

Table 5 Measured compressive properties of ECC

Concrete type	Mix proportion	Cubic compressive strength, f_{cu} (MPa)	Axial compressive strength, f_c (MPa)	f_c/f_{cu}	Elastic modulus, E_c (GPa)
1%-12-SSE	A-SSE	53.10	40.86	0.77	15.10
1.5%-12-SSE	B-SSE	41.11	29.34	0.71	12.80
2%-12-SSE	C-SSE	52.39	42.25	0.81	14.80
1.5%-18-SSE	D-SSE	49.42	38.33	0.78	14.61
1.5%-24-SSE	E-SSE	46.36	34.90	0.75	15.19
SSM	N-SSM	92.19	84.43	0.92	22.78
1.5%-12-ECC	B-ECC	45.92	37.94	0.83	12.17
MOR	N-MOR	77.95	70.30	0.90	17.44

may increase the porosity and internal initial defects of the cement matrix, resulting in a decrease in the stiffness of ECC to some extent. Huang et al. [31] revealed a dual role in ECC under compression: the fibers facilitate microcrack bridging, but the inherent hydrophobicity of PE impedes matrix compaction.

According to Table 5, under the same dosage of PE fiber, the elastic modulus of ECC showed an increasing trend with the increase of fiber length. The elastic modulus of ECC with 24 mm fiber was 1.18 times that of ECC mixed with 12 mm fiber, and 1.04 times that of ECC with 18 mm fiber. With the increase in fiber length, the growth of the elastic modulus of ECC became slower.

4.2.3 Stress–strain curve under uniaxial compression

The compressive stress–strain curves of ECC prisms are shown in Fig. 7. Unlike SSM and MOR, ECC specimens did not fail abruptly after reaching the peak load. Instead, the compressive stress of ECC exhibited a brief decline followed by a gradual deceleration in stress reduction rate. Concurrently, the number of surface cracks progressively increased with widening crack width. The incorporation of PE fiber caused concrete to show certain

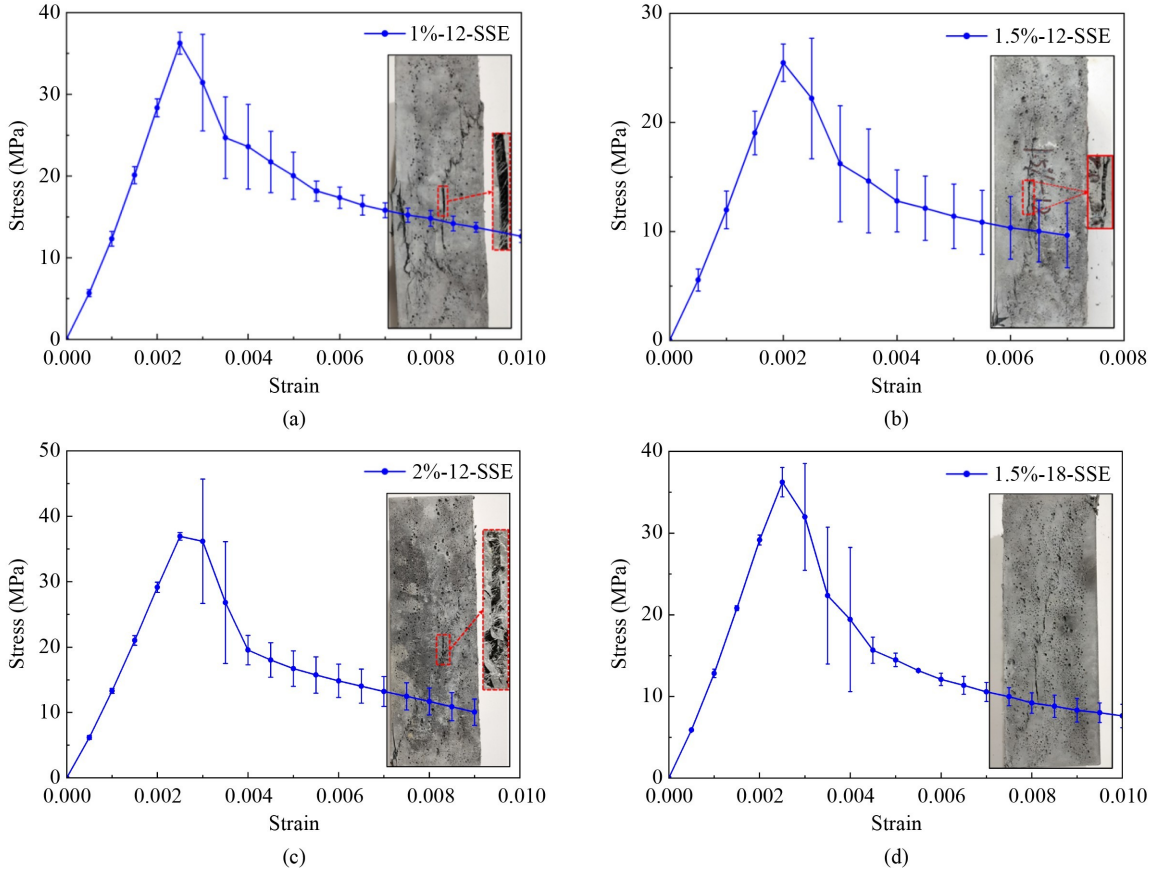

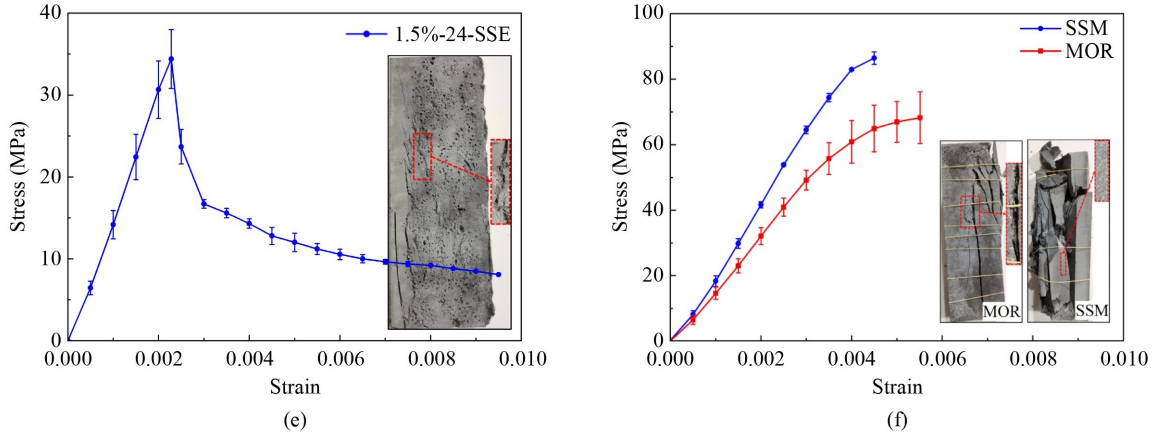

Fig. 7 Compressive stress–strain curves of ECC: (a) 1%-12-SSE; (b) 1.5%-12-SSE; (c) 2%-12-SSE; (d) 1.5%-18-SSE; (e) 1.5%-24-SSE; (f) SSM and MOR.

plastic characteristics during compressive failure.

4.2.4 Compressive toughness

Compressive toughness is an important mechanical property index of high ductile concrete. In this paper, the equivalent compressive toughness coefficient [41] was adopted to evaluate the compressive ductility of the ECC specimens. The equivalent compressive toughness coefficient indicates the deformation energy per unit volume of the specimen during uniaxial compression, quantifying the ability of materials to absorb energy and resist failure. The calculation formula of the equivalent compressive toughness coefficient is as follows

$$W_{cu} = \frac{\Omega_u}{Al}, \tag{3}$$

where W_{cu} is equivalent compressive toughness coefficient, Ω_u is the area enclosed by the load–deformation curve and the horizontal axis when the load drops to u times of the peak load (u = 0.85, 0.5, and 0.3 in this paper, shown in Fig. 8), A is the cross area of the specimen, and l is the height of the specimen.

According to the experimental results, the calculated equivalent compressive toughness coefficient is presented in Fig. 9.

As shown in Fig. 9(a), the equivalent compressive toughness coefficients $W_{0.85}$, $W_{0.5}$, and $W_{0.3}$ of 1%-12-SSE were 2.74, 2.08, and 2.19 times those of 1.5%-12-SSE, respectively. When the content of PE fiber increased from 1.5% to 2%, the equivalent compressive toughness coefficients $W_{0.85}$, $W_{0.5}$, and $W_{0.3}$ were 1.88, 1.38, and

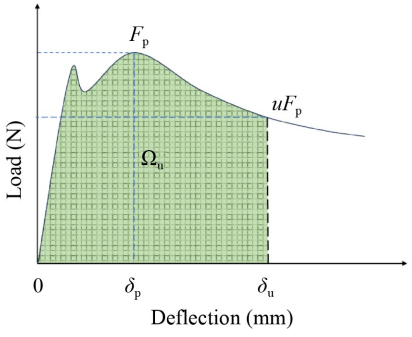

Fig. 8 Illustration of Ω_u for equivalent compressive toughness coefficient.

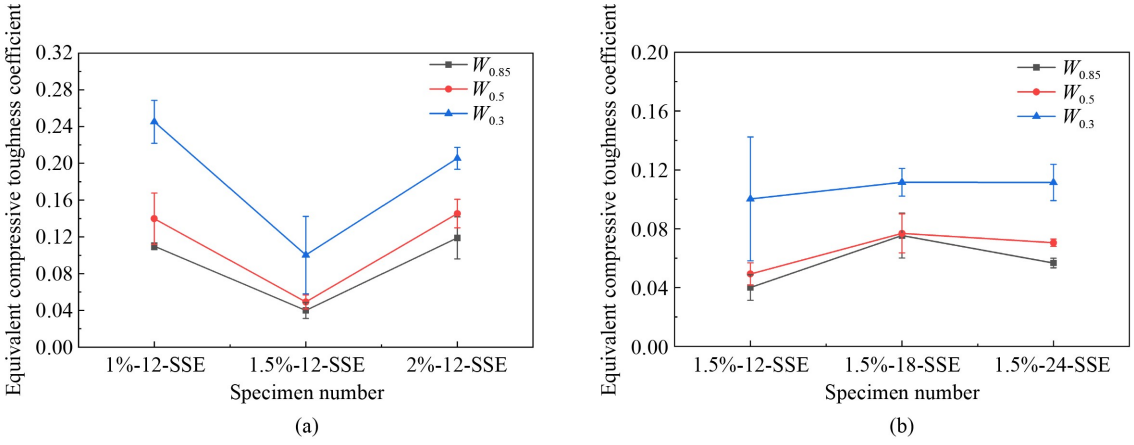

Fig. 9 Equivalent compressive toughness coefficient of ECC: (a) effect of fiber content; (b) effect of fiber length.

1.22 times those of the original, respectively. With the increase of fiber content, the equivalent compressive toughness coefficient of the prism became the lowest when the PE fiber content was 1.5%. The equivalent compressive toughness coefficient of concrete prisms with fiber content of 1% and 2% is not much different.

Figure 9(b) shows the effect of fiber length on the toughness of concrete. The equivalent compressive toughness coefficients $W_{0.85}$, $W_{0.5}$, and $W_{0.3}$ of 1.5%-18-SSE were 1.88, 1.38, and 1.22 times that of 1.5%-12-SSE, respectively. When the fiber length exceeded 18 mm, the equivalent compressive toughness coefficient of the specimen did not change much.

4.3 Flexural properties of engineered cementitious composites

Figure 10 illustrates the failure patterns of ECC specimens under four-point bending tests. The specimens with 0% fiber exhibited a single penetrating crack during testing, accompanied by minimal deflection deformation, demonstrating typical brittle fracture characteristics. In contrast, specimens with 1%–2% PE fiber displayed significantly enhanced plastic behavior at failure, attributed to the crack-arresting effect of fibers within the concrete matrix. These specimens developed multiple microcracks in addition to a dominant surface crack, with the distributed cracking pattern effectively delaying complete fracture penetration. The improved crack resistance mechanism resulted in substantially increased deformation capacity, as evidenced by greater specimen deflection and more gradual failure progression compared to the 0% fiber counterparts.

4.3.1 Flexural load–deflection response

Figure 10 also presents the bending load–deflection curves of ECC specimens with different PE fiber contents and lengths. Unlike the matrix, the load–deflection curves of ECC specimens can be divided into three stages [42,43].

1) Elastic stage. The load at this stage can be seen as

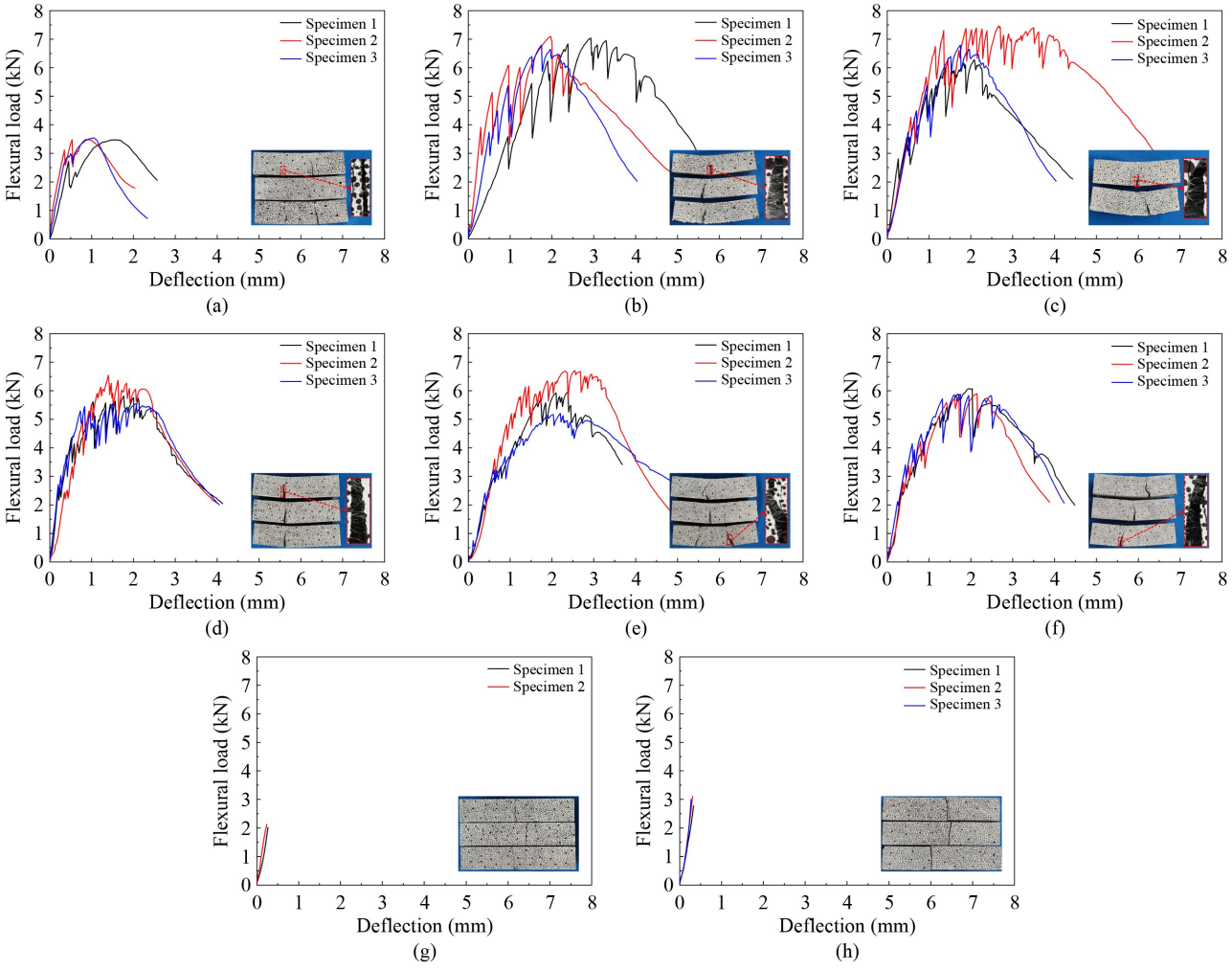

Fig. 10 Load–deflection curves of ECC under bending tests: (a) 1%-12-SSE; (b) 1.5%-12-SSE; (c) 1.5%-18-SSE; (d) 1.5%-24-SSE; (e) 2%-12-SSE; (f) 1.5%-12-ECC; (g) N-MOR; (h) N-SSM.

shared by the cement matrix and the PE fiber, and the load on the ECC specimen is linearly related to the deflection. Due to the existence of PE fibers in ECC, the first sudden drop of the load occurs at the first crack formation.

2) Strain hardening stage. After the initial cracking of the ECC, the cement matrix at the crack no longer bears the load, and the load is borne by the fiber between the cracks and the ECC at the uncracked part. As the test progresses, the deflection of the ECC specimen continues to increase, and the load on the specimen continues to increase in the form of multiple rises and drops, and multiple cracks appear on the surface of the specimen.

3) Strain softening stage. At this stage, the propagation of new cracks decelerates significantly, with the dominant mechanism shifting to the extension of pre-existing cracks. The fibers are either debonded or pulled out from the cement matrix, leading to a reduction in interfacial cohesion. The bearing capacity of the ECC specimen is gradually reduced, and the deflection of the specimen is increasing.

According to ASTM C1609-19 [44], the bending strength of the specimen in the four-point bending test can be calculated according to Eq. (4)

$$f_u = \frac{F_{max} L}{bh^2}, \tag{4}$$

where f_u is the bending strength of the specimen, F_{max} is the failure load of the specimen, L is the span between the two supports, b and h are the width and height of the specimen, respectively.

The flexural strength values of ECC specimens were obtained from Eq. (4) and are shown in Fig. 11. The flexural strength of SSM was 1.42 times that of MOR, and the flexural strength of 1.5%-12-SSE was 1.17 times that of 1.5%-12-ECC, indicating that seawater and sea sand have promoting effects on the flexural strength. Through the analysis of the compressive strength and flexural strength of ECC, it is found that seawater and sea sand have a positive effect on the compressive strength and flexural strength of fiber-reinforced concrete. Existing studies have demonstrated that the salts present in seawater and sea sand promote the early-age hydration of cement in ECC, thereby enhancing the density of the cement matrix, which in turn leads to improved compressive performance [45,46].

Figure 11 also shows that with the increase of fiber content, the flexural strength increased first and then decreased. When the PE fiber content was 1.5%, the

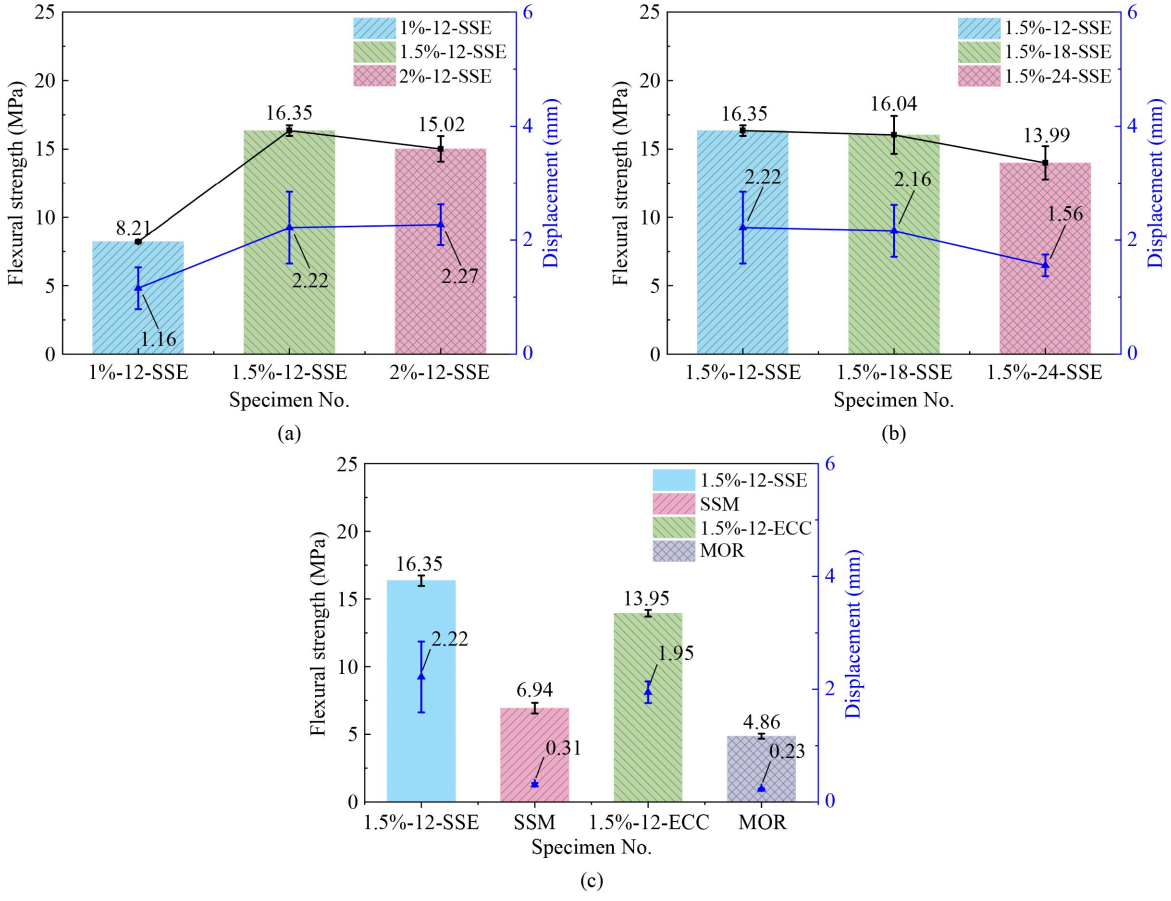

Fig. 11 Flexural strength of ECC: (a) flexural strength versus PE fiber content in ECC; (b) flexural strength versus PE fiber length in ECC; (c) flexural strength versus cement matrix composition in ECC.

flexural strength of ECC became the largest, which was 1.99 and 1.09 times that of ECC with fiber content of 1% and 2%, respectively. At low fiber content, the limited contact area between fibers and ECC resulted in minimal total cohesion. Consequently, the fiber bridging effect was negligible, leading to low flexural strength. At 2% fiber content, however, the increase in fibers also introduced more initial defects within the ECC matrix. At this point, the detrimental impact of these internal defects on flexural strength outweighed the beneficial fiber bridging effect, causing a reduction in flexural strength. Therefore, the optimal fiber content for achieving maximum flexural strength was 1.5%.

Figure 11 also presents the effect of fiber length on the flexural strength of ECC. As fiber length increased, the flexural strength of ECC gradually decreased. The decrease was more pronounced when the PE fiber length reached 24 mm. Specifically, the flexural strength of ECC specimens with 12 mm PE fibers was 1.02 and 1.17 times higher than those with 18 and 24 mm fibers, respectively. The primary reason for this reduction is that, at a constant fiber volume fraction, a longer fiber length results in fewer fibers contributing effectively to the bridging mechanism. Consequently, this reduces the overall flexural strength of the ECC. Meanwhile, fibers inhibit crack development primarily through pull-out or fracture. When fibers exceed an optimal length, their crack-bridging effectiveness diminishes compared to fibers of an appropriate length. Among the three fiber lengths tested (12, 18, and 24 mm), ECC with 12 mm fibers exhibited the highest flexural strength in this paper.

4.3.2 Analysis of flexural toughness

The flexural toughness can reflect the energy consumed by the specimen in the process of bending failure, serving as an important mechanical index of high ductility concrete such as ECC [47].

The flexural toughness indexes I_5, I_{10}, and I_{20}, as defined in ASTM C1018-97 [48], were used to evaluate the flexural toughness of ECC specimens. The deflection value at the first load drop in the rising part of the load–deflection curve was taken as the deflection value δ_{cr} corresponding to the initial cracking. The flexural toughness index of the specimen was obtained by calculating the ratio of the area enclosed by $3\delta_{cr}$, $5.5\delta_{cr}$, and $15.5\delta_{cr}$ to the load–deflection curve to the area enclosed by δ_{cr} and the load–deflection curve [42]. The calculation results are shown in Fig. 12.

Figure 12 shows that with the increase of PE fiber content from 1% to 2%, the flexural toughness of the ECC specimens also increased. When the fiber content was 1.5%, the flexural toughness of the ECC specimens grew slightly faster than that of the ECC specimens with 2% fiber content. When the deformation of the ECC specimens was less than $5.5\delta_{cr}$, the fiber length had little influence on the flexural toughness. When the deformation was beyond $5.5\delta_{cr}$, the flexural toughness of the ECC specimens increased significantly with the increase of fiber length.

5 Test results and analysis of shear performance of engineered cementitious composites beams

5.1 Failure mode and crack distribution

Figure 13 illustrates the failure mode of the ECC beam under shear when the applied load declined to 85% of the peak load. In contrast to the failure behavior of plain cement mortar beams (Figs. 13(a) and 13(b)), PE fiber reinforced ECC beams demonstrated distinct multi-cracking characteristics, featuring serrated principal diagonal cracks and rough fracture surfaces (Figs. 13(c)–13(q)).

Figures 13(c)–13(e) demonstrates the influence of fiber content on the failure mechanisms of ECC beams. Comparative analysis reveals that higher fiber content specimens exhibit significantly shorter crack propagation

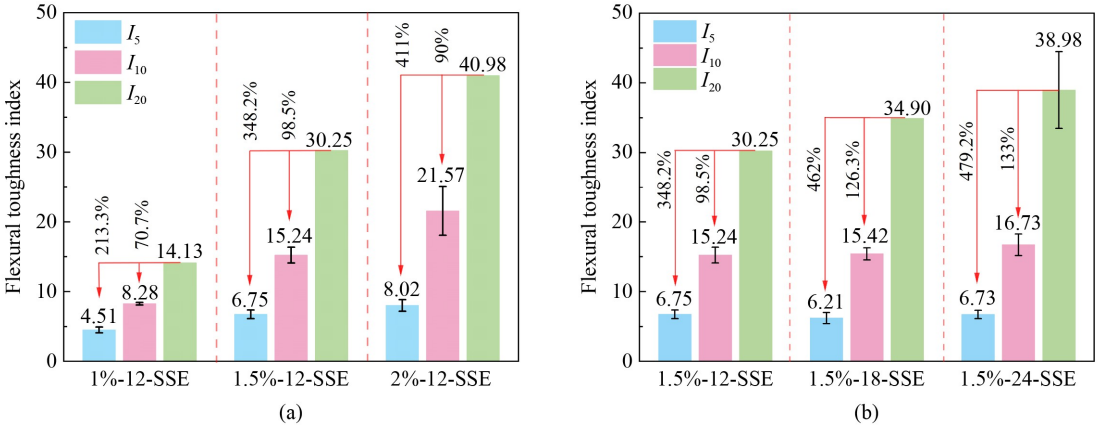

Fig. 12 Flexural toughness index of ECC specimens: (a) influence of fiber content; (b) influence of fiber length.

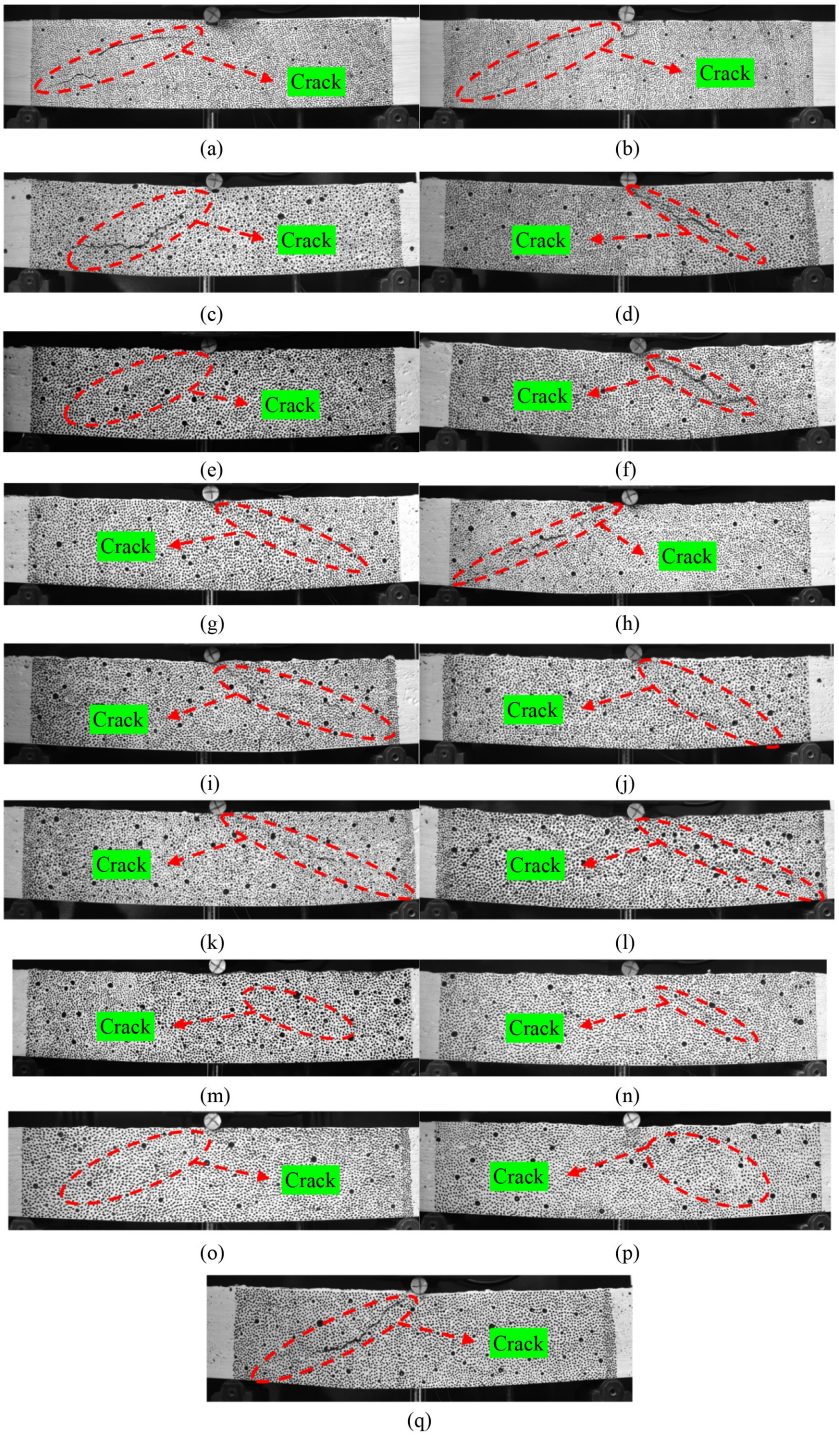

Fig. 13 Failure modes of ECC beams under shear: (a) SSM; (b) MOR; (c) S12(8)-2-A-SSE; (d) S12(8)-2-C-SSE; (e) S12(8)-2-B-SSE; (f) S12(8)-2-D-SSE; (g) S12(8)-2-E-SSE; (h) S12(8)-3-B-SSE; (i) S16(8)-2-B-SSE; (j) S16(10)-2-B-SSE; (k) G12-2-B-SSE; (l) G16-2-B-SSE; (m) G12-3-B-SSE; (n) H12-2-B-SSE; (o) H16-2-B-SSE; (p) H12-3-B-SSE; (q) S12(8)-2-B-ECC.

length. The experimental evidence confirmed that increasing fiber content effectively constrains crack development, with optimal crack inhibition observed at 1.5% PE fiber content. This trend aligns with existing literature, whereby a higher PE fiber volume fraction improves the fiber bridging force, thereby restricting crack development and resulting in narrower cracks [32].

Figures 13(e)–13(g) illustrates the dependence of the failure mode of ECC beams on the fiber length. ECC beams with 12 and 24 mm fibers demonstrated finer and more uniformly distributed cracking patterns than those shown in Fig. 13(f). The experimental results confirmed that fiber lengths of 12 and 24 mm effectively restrained crack propagation in ECC beams. An increase in PE fiber

length enhances interfacial bonding with the cement matrix. Huang's analysis of ECC cracks identified two primary failure modes: fiber pull-out and fiber rupture [32]. As fiber length increases, the proportion of fibers that rupture rises, which contributes to improved control over crack development. Furthermore, at a constant fiber volume fraction, ECC reinforced with 12 mm fibers contains a greater number of discrete fibers, leading to more effective crack control during beam cracking. Consequently, the crack width in ECC beams with 12 and 24 mm fibers is smaller than that in beams containing 18 mm fibers.

DIC analysis was performed to further investigate the crack distribution and propagation in ECC beams; results are presented in Fig. 14. Cracking initiation occurred at the beam's tension surface, manifesting as vertically oriented flexural cracks. With increasing applied load, the vertical flexural cracks propagated obliquely toward the loading point, while new diagonal cracks rapidly developed. This crack evolution demonstrated the multiple cracking behavior of the ECC beam. Figure 14 illustrates that the failure modes of the SS-ECC beams are predominantly flexural-shear.

Figures 14(c)–14(e) demonstrates that increased fiber content enhanced the multiple cracking behavior of ECC beams, as evidenced by the more pronounced crack distribution patterns. Figures 14(e)–14(g) illustrates the influence of fiber length on crack propagation in ECC beams. The results show that reducing fiber length from 24 to 12 mm yielded a more uniform crack distribution. Furthermore, ECC beams incorporating 12 and 18 mm PE fibers exhibited superior strain distribution homogeneity.

Figures 14(e), 14(h)–14(p) show that ECC beams reinforced with SFCB and HRB 400 bars exhibited slower crack propagation rates under identical loading conditions compared to GFRP-reinforced specimens. This difference may be attributed to the variation in the elastic

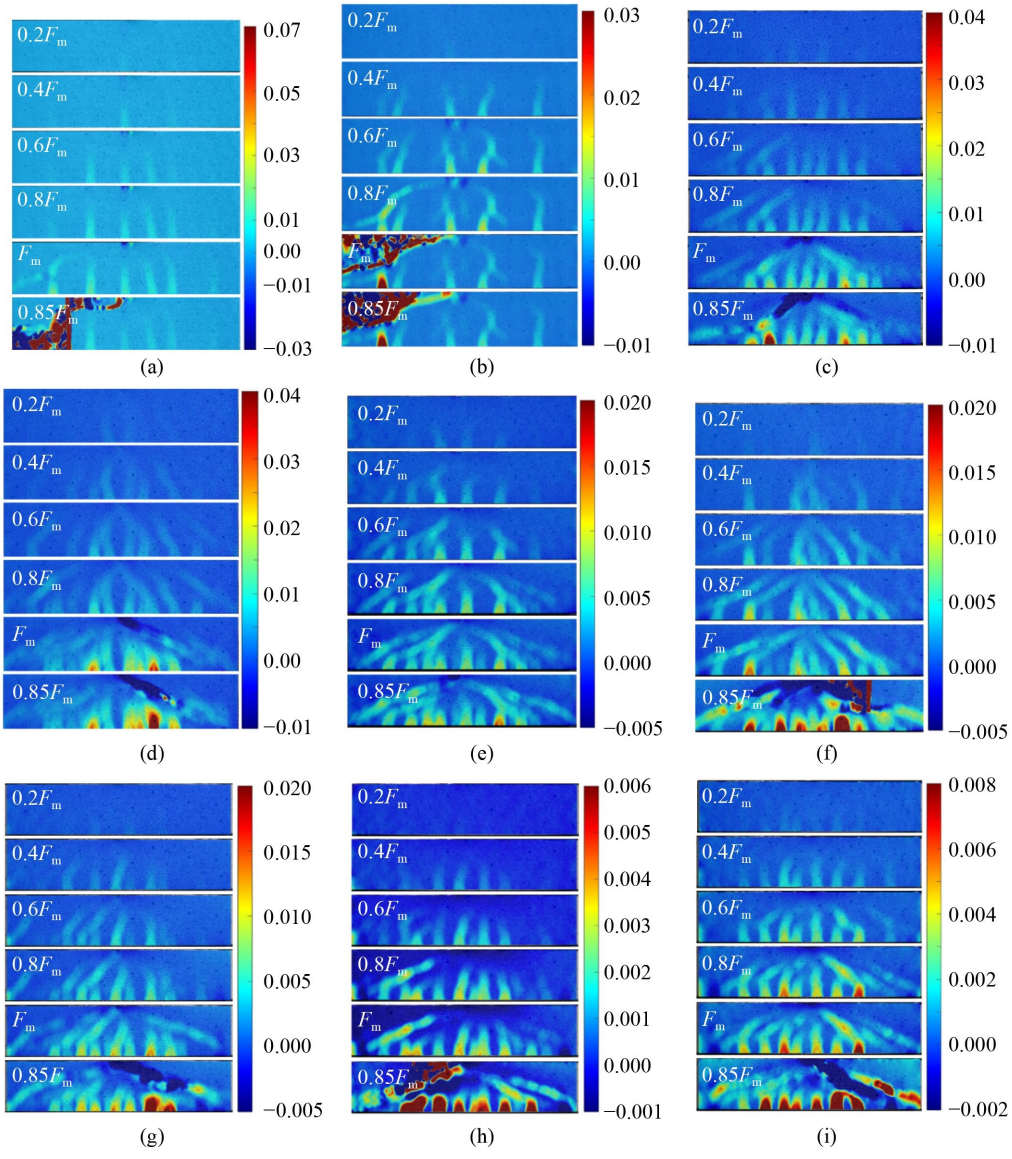

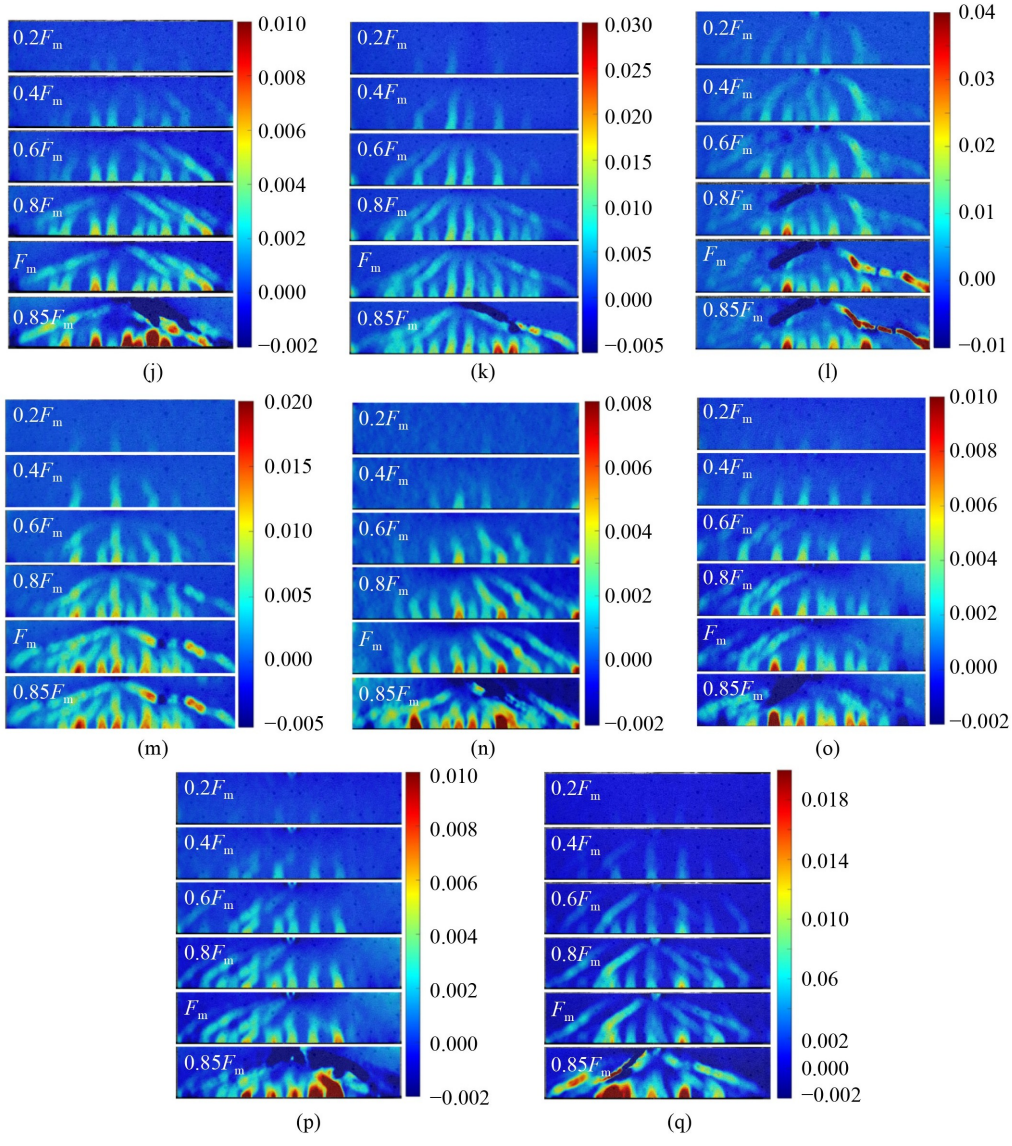

Fig. 14 Crack development analysis of ECC beams based on the DIC method: (a) SSM; (b) MOR; (c) S12(8)-2-A-SSE; (d) S12(8)-2-C-SSE; (e) S12(8)-2-B-SSE; (f) S12(8)-2-D-SSE; (g) S12(8)-2-E-SSE; (h) S12(8)-3-B-SSE; (i) S16(8)-2-B-SSE; (j) S16(10)-2-B-SSE; (k) G12-2-B-SSE; (l) G16-2-B-SSE; (m) G12-3-B-SSE; (n) H12-2-B-SSE; (o) H16-2-B-SSE; (p) H12-3-B-SSE; (q) S12(8)-2-B-ECC.

modulus of reinforcement. Specifically, lower modulus reinforcement resulted in greater deformation and reduced bond strength at the reinforcement-matrix interface [49]. The comparative analysis of Figs. 14(e), 14(h)–14(m) reveals that crack propagation can be effectively restrained by increasing reinforcement quantity, whereas enlarging reinforcement cross-sectional area tends to promote crack development.

5.2 Shear load–deflection curves

Figures 15–17 present the shear load–displacement curves of the ECC specimens. Figure 15 shows that the initial stiffness of the load–deflection curve of the ECC beam with HRB 400 and SFCB bars did not change much with the increase of the reinforcement ratio. When GFRP bars were used, the initial stiffness of the load–deflection curve increased with the increase in the reinforcement ratio. When different reinforcements were used, the initial stiffness of the load–deflection curve of the ECC beam is consistent with the change trend of the elastic modulus of the reinforcement, as shown in Fig. 16. Figure 17 shows that with the increase in the fiber content, the initial stiffness of the load–deflection curve of the ECC beam also increased. The fiber length had a limited effect on the load–deflection curve of the ECC beam.

5.3 Shear capacity of engineered cementitious composites beams

5.3.1 Effect of reinforcement ratio on shear capacity of engineered cementitious composites beams

The shear performance of ECC beams is summarized and

listed in Table 6, and illustrated in Fig. 18. With the increase of the GFRP reinforcement ratio, the shear capacity of ECC beams increased first and then decreased. As the GFRP reinforcement ratio increases (up to 4.6%), the total cross-sectional area of the bars crossing the diagonal cracks also increases. This enhances the confinement effect on the ECC matrix, thereby improving the shear capacity of the SS-ECC beams. Beyond a 4.6% GFRP reinforcement ratio, the resultant reduction in bar spacing and the inherently low elastic modulus of GFRP adversely affect the bond performance, leading to diminished shear capacity [23]. The shear capacity of ECC beams reinforced with HRB 400 rebars increased with the increase of reinforcement ratio. Unlike GFRP bars, HRB 400 bars exhibit a higher elastic modulus and develop a stronger interfacial bond with ECC. This synergistic effect contributes to more effective deformation control in the SS-ECC, which in turn leads to higher shear capacity [50]. The study indicates that increasing the SFCB reinforcement ratio does not markedly improve shear capacity but does substantially enhance the shear ductility of SS-ECC beams. Meanwhile, the shear capacity of S16(10)-2-B-SSE was 3.87% higher than that of S16(8)-2-B-SSE by increasing

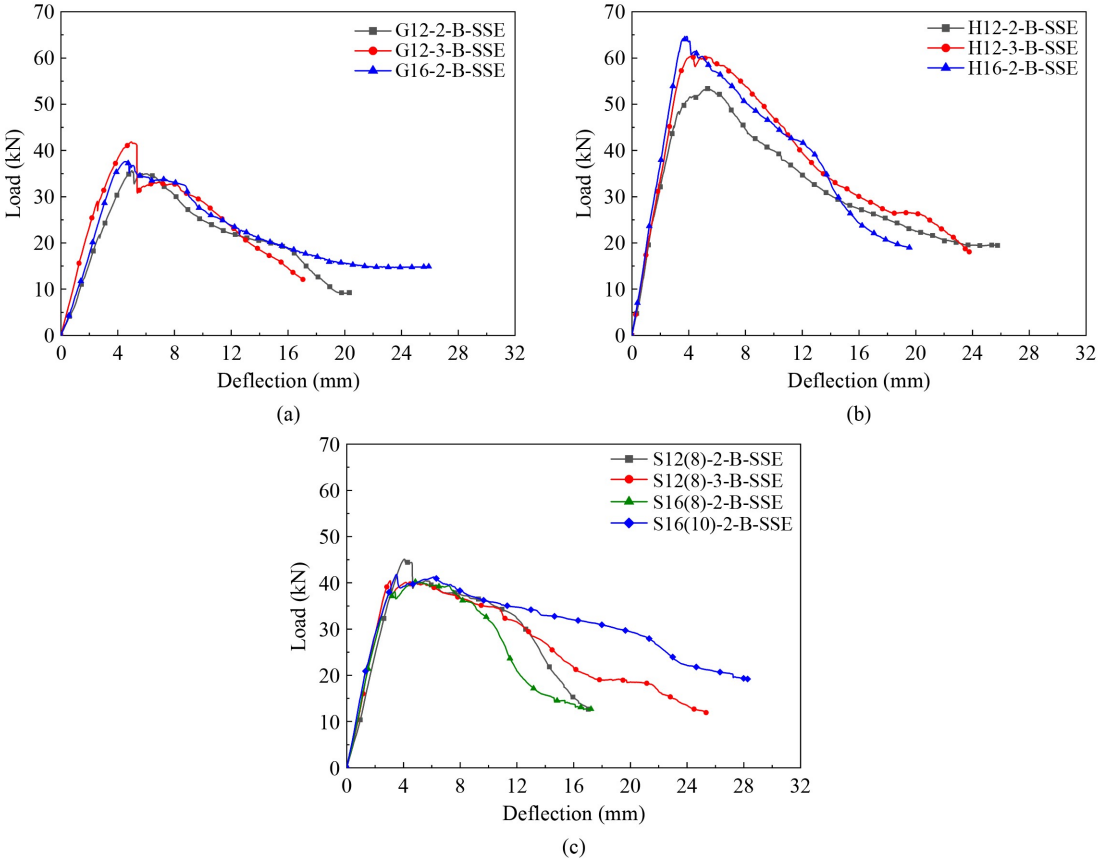

Fig. 15 Load–deflection curves of ECC beams with different reinforcement ratios: (a) GFRP; (b) HRB400; (c) SFCB.

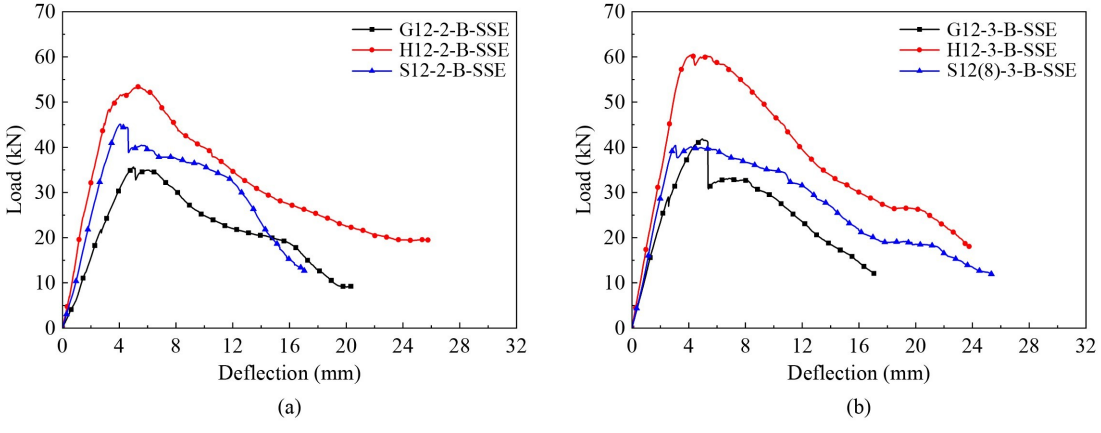

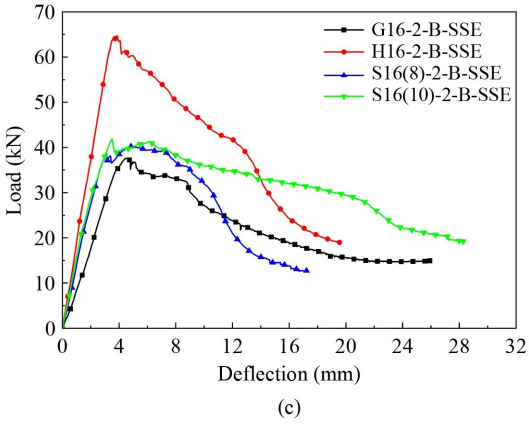

Fig. 16 Load–deflection curves of ECC beams with different reinforcement: (a) 3.0% reinforcement ratio; (b) 4.6% reinforcement ratio; (c) 5.6% reinforcement ratio.

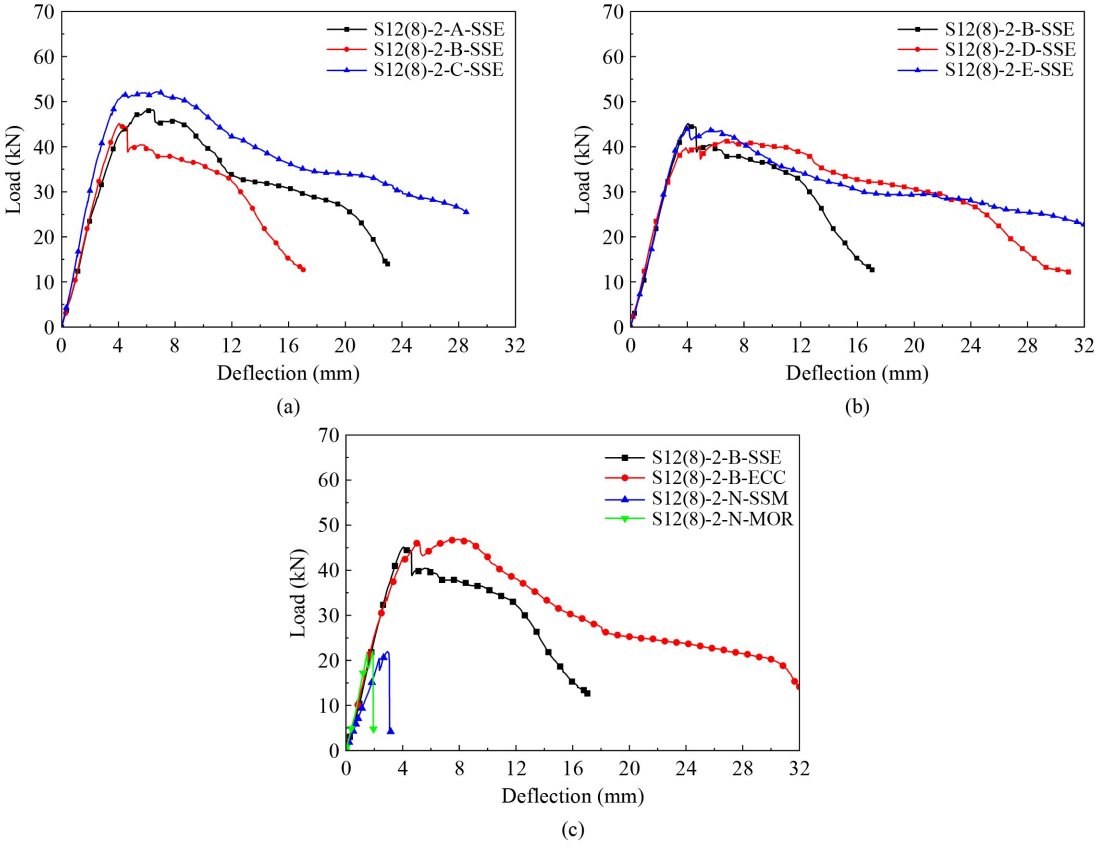

Fig. 17 Load–deflection curves of ECC beams with different mixes: (a) fiber content; (b) fiber length; (c) cement matrix.

the cross-sectional area of steel wrapped in SFCB bars. This means increasing the diameter of SFCB rebars may improve the shear capacity of ECC beams.

5.3.2 Effect of reinforcement type on shear capacity of engineered cementitious composites beams

The effects of different reinforcement on the shear performance of ECC beams are also shown in Table 6 and Fig. 18. When the reinforcement ratio was 3.06%, the shear capacity of H12-2-B-SSE was 49.9% and 18.4% higher than that of G12-2-B-SSE and S12(8)-2-B-SSE, respectively. When the reinforcement ratio was 4.58%, the shear capacity of H12-3-B-SSE was 44.3% and 49.4% higher than that of G12-3-B-SSE and S12(8)-3-B-SSE, respectively. When the reinforcement ratio was 5.58%, the shear capacity of H16-2-B-SSE was 72%, 60.6%, and 54.6% higher than that of G16-2-B-SSE, S16(8)-2-B-SSE and S16(10)-2-B-SSE, respectively.

Under each reinforcement ratio, due to the high elastic modulus of HRB400 rebar, the shear capacity of the ECC beams was greatly improved. However, in seawater and

Table 6 Shear performance of ECC beams

Specimen	Peak load, F_m (kN)	Peak deflection, Δ_m (mm)	Ultimate deflection, Δ_u (mm)	Yield deflection, Δ_y (mm)	Ductility factor, μ	Failure mode
S12(8)-2-N-SSM	21.95	2.93	3.06	2.44	1.25	shear
S12(8)-2-N-MOR	22.03	1.89	1.93	1.68	1.15	shear
S12(8)-2-A-SSE	48.14	6.45	9.85	4.50	2.19	shear–tension
S12(8)-2-C-SSE	52.16	6.71	11.13	3.72	2.99	flexural–shear
S12(8)-2-B-SSE	45.13	4.06	6.59	3.79	1.74	flexural–shear
S12(8)-2-D-SSE	41.41	6.72	13.54	3.64	3.72	shear–tension
S12(8)-2-E-SSE	44.19	4.03	9.60	3.64	2.64	shear–tension
S12(8)-3-B-SSE	40.43	3.06	10.76	2.87	3.74	flexural–shear
S16(8)-2-B-SSE	40.27	4.91	9.16	3.15	2.91	flexural–shear
S16(10)-2-B-SSE	41.83	3.51	10.72	2.98	3.59	flexural–shear
G12-2-B-SSE	35.65	5.01	8.03	4.67	1.72	flexural–shear
G16-2-B-SSE	37.60	4.52	8.84	4.20	2.11	flexural–shear
G12-3-B-SSE	41.84	4.98	8.42	3.93	2.14	flexural–shear
H12-2-B-SSE	53.44	5.37	7.83	3.56	2.20	flexural–shear
H16-2-B-SSE	64.69	3.88	6.67	3.47	1.92	flexural–shear
H12-3-B-SSE	60.38	4.15	8.75	3.57	2.45	flexural–shear
S12(8)-2-B-ECC	46.86	7.87	11.01	4.29	2.57	flexural–shear

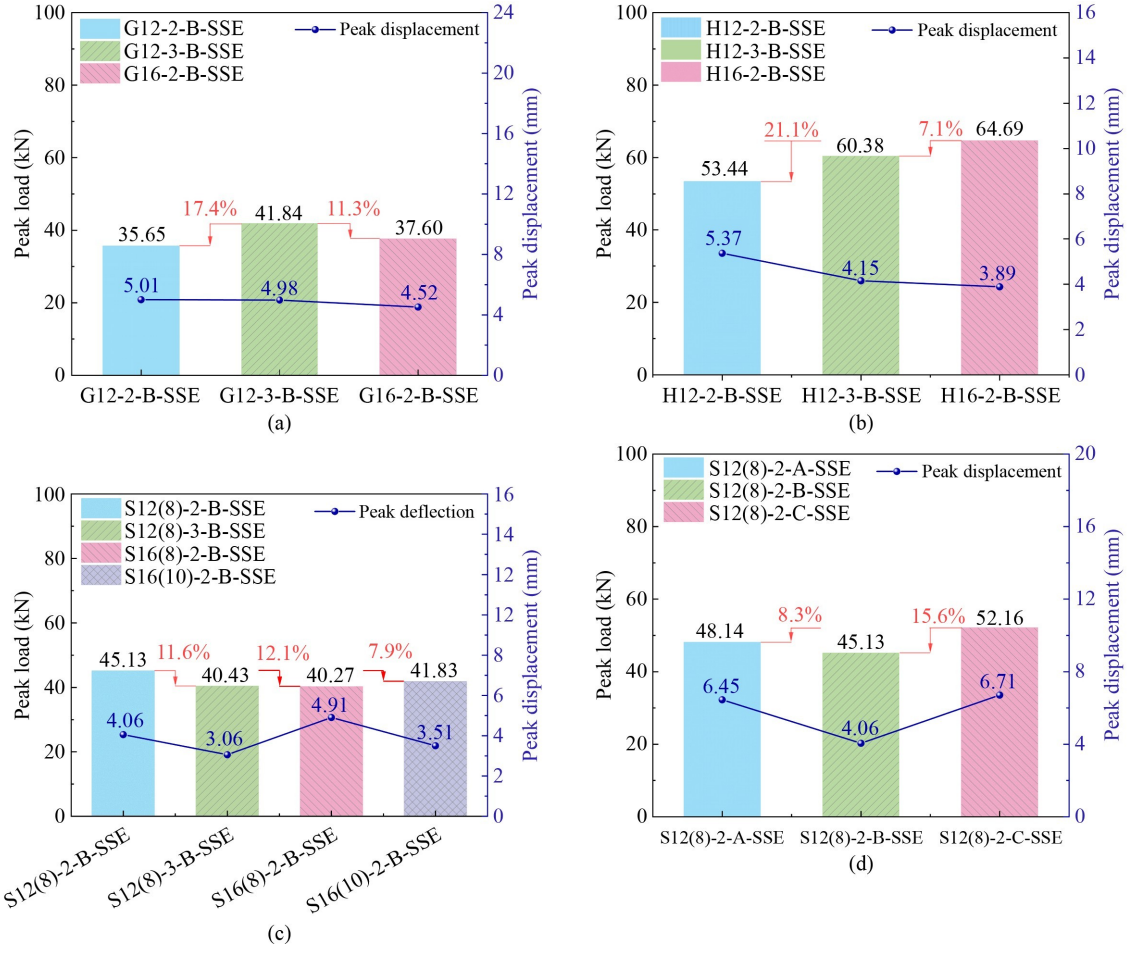

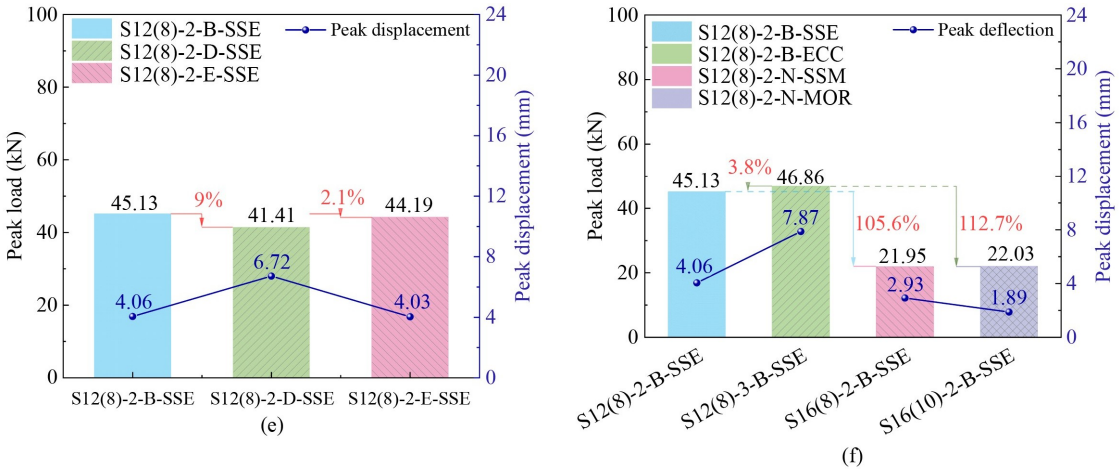

Fig. 18 Influence of different variables on shear capacity of ECC beams: (a) GFRP; (b) HRB400; (c) SFCB; (d) fiber content; (e) fiber length; (f) cement matrix.

sea sand concrete, steel bars can be easily corroded. SFCB bars cannot only make the ECC beams have better stiffness and bearing capacity, but also can effectively resist the steel corrosion induced by seawater and sea sand.

5.3.3 Effect of fiber content and length on shear capacity of engineered cementitious composites beams

The effect of fiber content on the shear capacity of ECC beams is shown in Fig. 18(d). With the increase of fiber dosage, the shear capacity of ECC beams decreased first and then increased, and reached the maximum when the fiber content was 2%, which is 8.36% and 15.57% higher than that of concrete beams with fiber content of 1% and 1.5%, respectively.

Figure 18(e) presents the effect of fiber length on the shear capacity of ECC beams. When the fiber length was 12 mm, the bearing capacity of ECC beams reached the maximum value, which was 8.99% and 2.14% higher than that of ECC beams with fiber length of 18 and 24 mm, respectively. Under the same fiber content, when the fiber length was 12 mm, the number of fibers that played a bridging role in the ECC was larger than that of the other two fibers. The fiber bridging effect improved and enhanced the shear capacity of the ECC specimens.

As shown in Fig. 18(f), the shear capacity of S12(8)-2-B-SSE and S12(8)-2-B-ECC was 2.05 and 2.13 times that of S12(8)-2-N-SSM and S12(8)-2-N-MOR, respectively. This means seawater and sea sand did not reduce the shear capacity of the specimens, and PE fiber significantly improved the shear capacity. Therefore, sea sand and seawater can be used in ECC to alleviate the shortage of freshwater and river sand.

5.4 Shear ductility of engineered cementitious composites beams

The ductility coefficient was used to calculate the shear ductility of ECC specimens. The initial yield point was determined by the equal energy method [51–53]. The calculation formula of the shear ductility coefficient is as follows

$$\mu = \frac{\Delta_u}{\Delta_y}, \tag{5}$$

where μ is the shear ductility coefficient, Δ_u is the displacement at 85% of the peak load in the descending section of the load–displacement curve, Δ_y is the displacement corresponding to the initial yield point.

The shear ductility values of ECC specimens are shown in Table 6. When the reinforcement ratio was not more than 4.58%, the ductility of each ECC specimen showed an upward trend with the increase of the reinforcement ratio. When the reinforcement ratio exceeded 4.58%, the ductility of the concrete specimen decreased, but the ECC specimens using SFCB bars still had good ductility. When the reinforcement ratio was 3.06%, the shear ductility coefficient of the H12-2-B-SSE specimen was 1.28 and 1.26 times that of G12-2-B-SSE and S12(8)-2-B-SSE, respectively. When the reinforcement ratio was 4.58%, the shear ductility coefficient of the specimen S12(8)-3-B-SSE was 1.75 and 1.52 times that of G12-3-B-SSE and H12-3-B-SSE, respectively. The analysis shows that when the reinforcement ratio was appropriate, SFCB and HRB 400 rebars significantly improved the shear ductility of the specimens compared with GFRP bars. Under the same reinforcement ratio, the shear ductility coefficient of S16(10)-2-B-SSE is 1.23 times that of S16(8)-2-B-SSE.Therefore, the shear ductility of the ECC specimen can be further increased by appropriately increasing the steel area inside the SFCB rebar.

With the increase of fiber content, the shear ductility coefficient of the specimens showed an upward trend and reached a maximum when the fiber content was 2%. The shear ductility coefficient of S12(8)-2-C-SSE was 1.36

and 1.72 times that of S12(8)-2-A-SSE and S12(8)-2-B-SSE, respectively. When the fiber length increased from 12 to 24 mm, the ductility coefficient reached a maximum when the fiber length was 18 mm. The shear ductility coefficient of S12(8)-2-D-SSE was 2.13 and 1.41 times that of S12(8)-2-B-SSE and S12(8)-2-E-SSE, respectively.

It shows that the shear ductility of the specimens can be significantly improved by adjusting the reinforcement ratio of SFCB bars and the area ratio of internal steel. Meanwhile, shear ductility coefficient of S12(8)-2-C-SSE and S12(8)-2-D-SSE was 16.48% and 44.82% higher than that of S12(8)-2-B-ECC, respectively. Compared with specimens with freshwater and river sand, the shear ductility of SS-ECC specimens can be increased by changing the reinforcement ratio, fiber content, and fiber length.

6 Calculation of shear capacity

6.1 Development of shear capacity model for engineered cementitious composites beams

The ECC beam without web reinforcement bears shear load mainly through three parts: cement matrix, longitudinal reinforcement, and fibers at the critical oblique crack.

According to ACI 440.1R-15 [54], the shear contributions from the cementitious matrix and the longitudinal reinforcement can be determined as follows:

$$V_w = V_c + V_d = 0.4\sqrt{f_c'}bh_0\left(\sqrt{2\rho_f n_f + (\rho_f n_f)^2} - \rho_f n_f\right), \quad (6)$$

where V_w is the shear capacity of concrete beams without web reinforcement, f_c' is the compressive strength, b is the width of the concrete beam, h_0 is the effective height of the concrete beam, ρ_f is the longitudinal reinforcement ratio, n_f is the ratio of the elastic modulus of longitudinal reinforcement to concrete.

In accordance with the design provisions of CSA S806-12 [55], the shear strength contributions from the cementitious matrix and the longitudinal reinforcement are evaluated separately as follows

$$V_w = V_c + V_d = 0.05\phi_c k_a k_m k_r (f_c')^{\frac{1}{3}} bh_v, \quad (7)$$

where ϕ_c is resistance factor for concrete, take 0.65 for ϕ_c, k_a is coefficient taking into account the effect of arch action on member shear strength, $1 \leqslant k_a = \dfrac{2.5V_f h_0}{M_f} \leqslant 2.5$, k_m is coefficient taking into account the effect of moment at section on shear strength, $k_m = \sqrt{\dfrac{V_f h_0}{M_f}} \leqslant 1$, k_r is coefficient taking into account the effect of reinforcement rigidity on its shear strength, $k_r = 1 + (E_f\rho_f)^{\frac{1}{3}}$, E_f is modulus of elasticity of FRP reinforcement, h_v is effective shear depth, taken as the greater of $0.9h_0$ or $0.72h$.

Through the specification GB 50608-2020 [56], the contribution of cement matrix and longitudinal reinforcement to shear capacity V_w can be obtained as follows

$$V_w = V_c + V_d = 0.86 f_t b h_0\left(\sqrt{2\rho_f n_f + (\rho_f n_f)^2} - \rho_f n_f\right). \quad (8)$$

In Eq. (8), f_t represents the tensile strength of concrete.

By integrating the derived relationships for ECC tensile strength f_t and fiber characteristic parameters λ (Eqs. (1) and (8)), this study established a shear capacity formulation that incorporates the influence of fiber characteristics for ECC beams

$$V = a f_{t0}(1 + \alpha\lambda) b h_0\left(\sqrt{2\rho_f \eta_f + (\rho_f \eta_f)^2} - \rho_f \eta_f\right). \quad (9)$$

Furthermore, this study adopts the tensile−compressive strength relationship defined in the Chinese code GB/T 50010-2010 [57], as shown in Eq (10)

$$f_{t0} = 0.395 f_{cu}^{0.55}. \quad (10)$$

Combining Eqs. (9) and (10) gives

$$V = 0.395 a f_{cu}^{0.55}(1 + \alpha\lambda) b h_0\left(\sqrt{2\rho_f \eta_f + (\rho_f \eta_f)^2} - \rho_f \eta_f\right). \quad (11)$$

As evidenced in Table 6, the failure mode of beams S12(8)-2-A-SSE, S12(8)-2-D-SSE, and S12(8)-2-E-SSE was shear-tension failure. Formula fitting was not performed on SSE-ECC beams that failed in shear-tension. According to Eq. (1), α is 0.13716. A linear regression was conducted, as shown in Fig. 19. a is 0.91692 ± 0.03 with R^2 = 0.985. Figure 19 presents the comparison of experimental results for the shear capacity of ECC beams along with the predictions from Eqs. (6)–(8) and (11). The corresponding mean ratios of prediction to experimental value were 0.48 ± 0.24, 0.37 ± 0.19, 0.33 ± 0.05, and 1.04 ± 0.14, respectively. Compared to alternative models, Eq. (11), which is based on GB 50608-2020 [56], shows improved agreement with the experimental data obtained in this work.

6.2 Validation against additional experimental results

To further validate the reliability of Eq. (11), supplementary experimental data comprising the shear capacities of 22 additional stirrup-free ECC beams were collected from the existing literature. Table 7 presents the ratio of experimental to calculated shear capacity (V_e/V_c) for ECC beams. The predictions obtained from Eq. (11) show good agreement with experimental results from independent studies, with V_e/V_c ratios ranging from 0.78 to 1.17. These findings demonstrate the reasonable

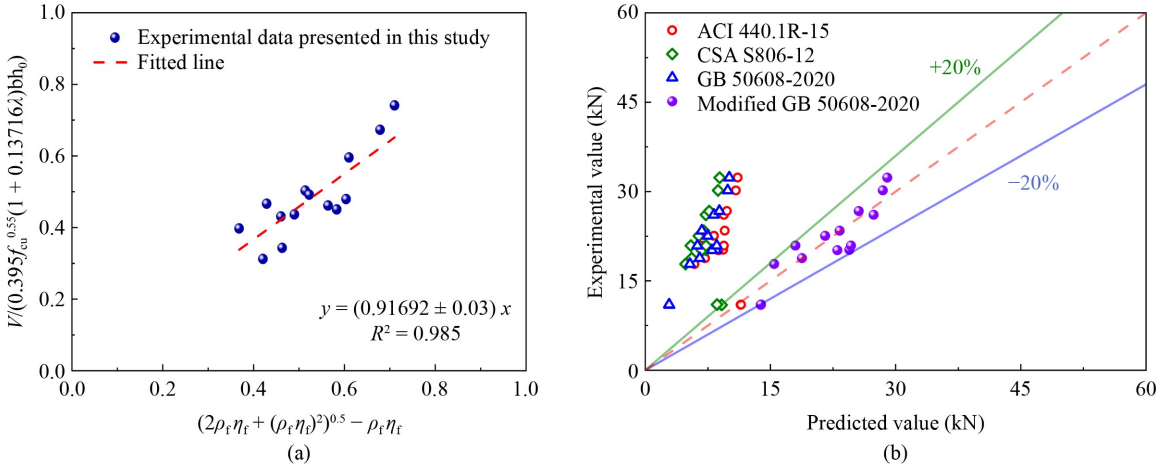

Fig. 19 Relationship between fiber characteristic value and shear capacity: (a) relationship between fiber characteristic value and shear capacity; (b) comparison of test and calculated values of shear capacity of ECC beams.

Table 7 Comparison of experimental (V_e) and calculated (V_c) shear capacity

Specimen	$b \times h_0$	λ	f_{cu}	ρ_f	V_e	V_c	V_c/V_e
D-U3 [58]	120 × 147	6	46.22	2.28%	58.39	51.22	0.88
D-U4 [58]	120 × 147	6	46.59	2.28%	43.77	51.36	1.17
E-U3 [58]	120 × 146	6	45.73	3.25%	66.6	56.41	0.84
E-U4 [58]	120 × 146	6	45.73	3.25%	50.61	56.41	1.11
F-U3 [58]	120 × 149	6	47.76	4.25%	70.03	63.05	0.90
F-U4 [58]	120 × 149	6	47.76	4.25%	62.67	63.05	1.01
0-L1.58-AD2.5 [59]	90 × 140	6.37	34.3	1.58%	36.3	31.27	0.86
0-L2.27-AD2.5 [59]	90 × 140	6.37	34.3	2.27%	36.3	34.97	0.96
0-L3.07-AD2.0 [59]	90 × 140	6.37	34.3	3.07%	37.8	38.05	1.01
0-L3.07-AD2.5 [59]	90 × 140	6.37	34.3	3.07%	33.2	38.05	1.15
0-L3.07-AD3.0 [59]	90 × 140	6.37	34.3	3.07%	32.4	38.05	1.17
2-L1.58-AD2.5 [59]	90 × 140	6.37	40.3	1.58%	29.3	34.27	1.17
2-L2.27-AD2.5 [59]	90 × 140	6.37	40.3	2.27%	41.2	38.31	0.92
2-L3.07-AD2.0 [59]	90 × 140	6.37	40.3	3.07%	50.4	41.68	0.83
2-L3.07-AD2.5 [59]	90 × 140	6.37	40.3	3.07%	43.1	41.68	0.97
2-L3.07-AD3.0 [59]	90 × 140	6.37	40.3	3.07%	36.2	41.68	1.15
MN4 [60]	200 × 331	6	84.94	2.1%	286.4	225.01	0.79
MN5 [60]	200 × 331	6	78.10	2.6%	295.3	231.47	0.78
MN6 [60]	200 × 331	6	71.39	3.2%	289.5	236.12	0.82
LN4 [60]	200 × 331	6	93.54	2.1%	302.4	237.28	0.79
LN5 [60]	200 × 331	6	73.92	2.6%	261.4	224.58	0.86
LN6 [60]	200 × 331	6	74.81	3.2%	302	242.27	0.80

applicability of Eq. (11) to external test data.

7 Conclusions

The use of SFCB reinforcement in SS-ECC structures presents a dual advantage: enhancing the structural strength and offering a sustainable solution to the scarcity of freshwater and river sand for coastal construction. This study investigates the effects of PE fiber volume fraction (0%, 1%, 1.5%, and 2%) and fiber length (12, 18, and 24 mm) on the strength and toughness of SS-ECC. The shear performance of 17 concrete beams was tested to evaluate the impact of key design parameters on the shear behavior of stirrup-free SS-ECC beams. The parameters included the type (HRB 400, GFRP, SFCB) and ratio

(3%, 4.6%, 5.6%) of longitudinal reinforcement, and the volume fraction (0%–2%) and length (12–24 mm) of PE fibers. The main findings derived from this experimental investigation can be summarized as follows.

1) The mechanical properties of SS-ECC are highly dependent on PE fiber parameters. While a fiber content of 1.5% and a length of 24 mm maximize tensile strength, the same content with 12 mm fibers optimizes flexural strength. Although PE fibers cause a marginal reduction in compressive strength, they profoundly enhance toughness and suppress brittle failure. SS-ECC showed a 12% larger tensile strength, and a 17% larger flexural strength, whereas a 10% lower compressive strength than ECC without seawater and sea sand.

2) For SFCB-reinforced SS-ECC beams without web reinforcement, PE fiber content and length have a limited effect on the ultimate shear capacity. However, they are critical for enhancing structural ductility. Increasing the fiber content from 1% to 2% and the fiber length from 12 to 24 mm can improve the shear ductility by over 35% and 50%, respectively.

3) SFCB reinforcement offers a favorable balance between strength and ductility. While beams with GFRP and SFCB rebars exhibit lower shear capacity than steel-reinforced beams due to their lower axial stiffness, increasing the inner steel cross-sectional area in the SFCB (e.g., from S16(8) to S16(10)) can simultaneously enhance both shear capacity (by 3.9%) and ductility coefficient (by 23.4%).

4) The proposed shear capacity model demonstrates good predictive capability across beams reinforced with steel, GFRP, and SFCB rebars. Its validation against external data sets (predicted-to-experimental ratios of 0.78–1.17) confirms its potential for practical application.

This study developed SFCB rebar reinforced SS-ECC beams for coastal structures, considering the shear performance. The test results can provide insights into the shear behavior of such beams, and contribute to the shear design of SFCB rebar reinforced SS-ECC beams without stirrups. Since the SS-ECC beam section was small-scaled in this paper, future studies are needed on the full-scale beams to better reveal the shear behavior.

Acknowledgements The authors would like to gratefully acknowledge the research grants from the National Natural Science Foundation of China (Grant Nos. 52408177 and 52378179), Qing Lan Project of Jiangsu Higher Education Institution, Postgraduate Research & Practice Innovation Program of Jiangsu Province (No. SJCX24-2079), and Postgraduate Research & Practice Innovation Program of Jiangsu Ocean University (No. KYCX2024-60).

Competing interests The authors declare that they have no competing interests.

References

1. Xiao J, Qiang C, Nanni A, Zhang K. Use of sea-sand and seawater in concrete construction: Current status and future opportunities. Construction & Building Materials, 2017, 155: 1101–1111
2. Dhondy T, Remennikov A, Shiekh M N. Benefits of using sea sand and seawater in concrete: A comprehensive review. Australian Journal of Structural Engineering, 2019, 20(4): 280–289
3. Bazli M, Li Y, Zhao X, Raman R K S, Bai Y, Al-Saadi S, Haque A. Durability of seawater and sea sand concrete filled filament wound FRP tubes under seawater environments. Composites. Part B, Engineering, 2020, 202: 108409
4. Yang J, Lu S, Wang J, Wang Z. Behavior of CFRP partially wrapped square seawater sea-sand concrete columns under axial compression. Engineering Structures, 2020, 222: 111119
5. Li Y, Liu W, Mi T, Ding X, Tang L, Xing F. Durability study of seawater and sea-sand concrete under the combined effects of carbonation and chloride redistribution. Journal of Building Engineering, 2024, 89: 109294
6. Li P, Li W, Sun Z, Shen L, Sheng D. Development of sustainable concrete incorporating seawater: A critical review on cement hydration, microstructure and mechanical strength. Cement and Concrete Composites, 2021, 121: 104100
7. Etxeberria M, Gonzalez-Corominas A, Pardo P. Influence of seawater and blast furnace cement employment on recycled aggregate concretes' properties. Construction & Building Materials, 2016, 115: 496–505
8. Etxeberria M, Fernandez J M, Limeira J. Secondary aggregates and seawater employment for sustainable concrete dyke blocks production: Case study. Construction & Building Materials, 2016, 113: 586–595
9. Ting M Z Y, Wong K S, Rahman M E, Selowara Joo M. Mechanical and durability performance of marine sand and seawater concrete incorporating silicomanganese slag as coarse aggregate. Construction & Building Materials, 2020, 254: 119195
10. Xie Q, Xiao J, Zong Z. Strength and microstructure of seawater and sea sand mortar after exposure to elevated temperatures. Construction & Building Materials, 2022, 322: 126451
11. Benny B, Bazli M, Rajabipour A, Arashpour M. Durability of tubular sea water sea sand concrete and fibre-reinforced polymer hybrid structures: Mechanisms and effective parameters: Critical overview and discussion. Construction & Building Materials, 2023, 366: 130206
12. Bazli M, Heitzmann M, Hernandez B V. Hybrid fibre reinforced polymer and seawater sea sand concrete structures: A systematic review on short-term and long-term structural performance. Construction & Building Materials, 2021, 301: 124335
13. Xie Q, Zhang H, Xiao J, Zong Z. Mechanical behavior and its variability analysis of fiber reinforced polymer rebars after high temperatures. Construction & Building Materials, 2023, 380: 131266
14. Mahroug M E M, Ashour A F, Lam D. Experimental response and code modelling of continuous concrete slabs reinforced with BFRP bars. Composite Structures, 2014, 107: 664–674
15. Han S, Zhou A, Ou J. Relationships between interfacial behavior

and flexural performance of hybrid steel-FRP composite bars reinforced seawater sea-sand concrete beams. Composite Structures, 2021, 277: 114672
16. Liang X, Peng J, Ren R. A state-of-the-art review: Shear performance of the concrete beams reinforced with FRP bars. Construction & Building Materials, 2023, 364: 129996
17. Liu S, Zhou Y, Zheng Q, Zhou J, Jin F, Fan H. Blast responses of concrete beams reinforced with steel-GFRP composite bars. Structures, 2019, 22: 200–212
18. Zhou Y, Zheng Y, Pan J, Sui L, Xing F, Sun H, Li P. Experimental investigations on corrosion resistance of innovative steel-FRP composite bars using X-ray microcomputed tomography. Composites. Part B, Engineering, 2019, 161: 272–284
19. Zhao D, Pan J, Zhou Y, Sui L, Ye Z. New types of steel-FRP composite bar with round steel bar inner core: Mechanical properties and bonding performances in concrete. Construction & Building Materials, 2020, 242: 118062
20. Ibrahim A I, Wu G, Sun Z, Cui H. Cyclic behavior of concrete columns reinforced with partially unbonded hybrid. Engineering Structures, 2017, 131: 311–323
21. Yan W, Zhang R, Sushant S, Ashour A, Fu S, Qiu L, Zhang Z, Ge W. Experimental investigation on fexural performance of UHPC beams reinforced with steel-FRP bars. Archives of Civil and Mechanical Engineering, 2024, 24(2): 132
22. Sun Y, Fu J, Sun Z, Zhang J, Wei Y, Wu G. Flexural behavior of concrete beams reinforced by partially unbonded steel-FRP composite bars. Engineering Structures, 2022, 272: 115050
23. Bai Y, Ma Q, Zhang Y, Jin X, Han S. Bond behavior and modeling of steel-FRP composite bars in engineered cementitious composites. Case Studies in Construction Materials, 2024, 20: e03320
24. Ge W, Wang Y, Ashour A, Lu W, Cao D. Flexural performance of concrete beams reinforced with steel-FRP composite bars. Archives of Civil and Mechanical Engineering, 2020, 20(2): 56
25. Zhou Y, Gao H, Hu Z, Qiu Y, Guo M, Huang X, Hu B. Ductile, durable, and reliable alternative to FRP bars for reinforcing seawater sea-sand recycled concrete beams: Steel/FRP composite bars. Construction & Building Materials, 2021, 269: 121264
26. Han S, Fan C, Zhou A, Ou J. Simplified implementation of equivalent and ductile performance for steel-FRP composite bars reinforced seawater sea-sand concrete beams: Equal-stiffness design method. Engineering Structures, 2022, 266: 114590
27. Han S, Fan C, Zhou A, Ou J. Shear behavior of concrete beams reinforced with corrosion-resistant and ductile longitudinal steel-FRP composite bars and FRP stirrups. Engineering Structures, 2023, 278: 115520
28. Yuan S, Qian W, Lu C, Manandhar G, Zhong X, Tong T. Shear capacity of sea-sand concrete beams reinforced with steel-BFRP composite bars and BFRP stirrups: Experimental investigation and calculation model. Structures, 2025, 82: 110670
29. Zhu J, Weng K, Huang B, Xu L Y, Dai J G. Ultra-high-strength engineered cementitious composites (UHS-ECC) panel reinforced with FRP bar/grid: Development and flexural performance. Engineering Structures, 2024, 302: 117193
30. Lao J, Huang B, Xu L, Khan M, Fang Y, Dai J G. Seawater sea-sand engineered geopolymer composites (EGC) with high strength and high ductility. Cement and Concrete Composites, 2023, 138: 104998
31. Huang B, Wu J, Yu J, Dai J G, Leung C K Y. High-strength seawater sea-sand engineered cementitious composites (SS-ECC): Mechanical performance and probabilistic modeling. Cement and Concrete Composites, 2020, 114: 103740
32. Huang B, Wu J, Yu J, Dai J G, Leung C K Y, Li V C. Seawater sea-sand engineered/strain-hardening cementitious composites (ECC/SHCC): Assessment and modeling of crack characteristics. Cement and Concrete Research, 2021, 140: 106292
33. Liao Q, Yu J, Shi T, Yu K, Su Y. Seawater sea-sand engineered cementitious composites contribution to shear performance of beams reinforced with BFRP bars. Composite Structures, 2023, 320: 117183
34. Liao Q, Yu J, Dong F, Su Y, Yu K. FRP bars reinforced seawater sea-sand engineered cementitious composites beams with various salinities: Shear behaviors and cost effectiveness. Journal of Building Engineering, 2024, 83: 108452
35. T/CCPA 7-2018. Fundamental Characteristics and Test Methods of Ultra-high Performance Concrete. Beijing: China Building Materials Federation, 2018
36. Blaber J, Adair B, Antoniou A. Ncorr: Open-source 2D digital image correlation matlab software. Experimental Mechanics, 2015, 55(6): 1105–1122
37. Sasania F, Nematzadeh M, Asadi M, Aminian A. Thermo-mechanical behavior of high-strength concrete with nylon granule aggregates: Experimental evaluation and predictive analysis. Civil Engineering and Applied Solutions, 2025, 1(1): 1–35
38. Shariati M, Pourteymuri M, Naghipour M, Toghroli A, Afrazi M, Shariati M, Aminian A, Nematzadeh M. Evolution of confinement stress in axially loaded concrete-filled steel tube stub columns: Study on enhancing urban building efficiency. Sustainability, 2024, 16(17): 7544
39. Wang J, Liu E, Li L. Multiscale investigations on hydration mechanisms in seawater OPC paste. Construction & Building Materials, 2018, 191: 891–903
40. Li Y, Zhu J, Wu Y. Effect of fiber on mechanical property of cementitious composite. Journal of Huazhong University of Science and Technology, 2017, 45(11): 57–61
41. Jiang S, Tao S, Yao W, Wu S, Cai T. Mechanical performance and size effect of engineered cementitious composite (ECC) subjected to uniaxial compression. Materials Review, 2017, 31(24): 161–168, 173 (in Chinese)
42. Wu H, Long G, Yang K, Zeng X, Tang Z. Effects of PE fiber and fine rubber particles on flexural toughness of foam concrete. Journal of Building Materials, 2024, 27(03): 206–214
43. Shang J, Zhao K, Zhang P, Guo W, Zhao T. Flexural behavior of plain concrete beams containing strain hardening cementitious composite layers with High-Volume fly ash. Construction & Building Materials, 2021, 286: 122867
44. ASTM. Standard Test Method for Flexural Performance of Fiber Reinforced Concrete (Using Beam with Third-Point Loading), ASTM C1609/C1609M-19. West Conshohocken, PA: ASTM, 2019
45. Wei J, Ke L, Wang P, Li W, Leung C K Y. Microstructure, mechanical properties and interaction mechanism of seawater sea-

sand engineered cementitious composite (SS-ECC) with Glass Fiber Reinforced Polymer (GFRP) bar. Composite Structures, 2024, 343: 118302

46. Das A K, Qi Y. High performance natural seawater coral sand ECC (HP-NSCS-ECC) in coastal conditions: Experimental characterization, microstructure, and sustainability. Construction & Building Materials, 2025, 499: 143860
47. Zhong G, Zhou Y, Xia Y. Stress–strain behavior of steel-polyviny alcohol hybrid fiber reinforced concrete under axial compression and tension. Engineering Mechanics, 2020, 37(S1): 111–120 (in Chinese)
48. ASTM. Standard Test method for Flexural Toughness and First-Crack Strength of Fiber Reinforced Concrete (Using Beam with Third-Point Loading), ASTM C 1018-97. West Conshohocken, PA: ASTM, 1997
49. Gomes T A, de Resende T L, Cardoso D C T. Shear-transfer mechanisms in reinforced concrete beams with GFRP bars and basalt fibers. Engineering Structures, 2023, 289: 116299
50. Xu L, Wang X, Pan J, Zhou J, Liu W. Bond behavior between steel-FRP composite bars and engineered cementitious composites in pullout conditions. Engineering Structures, 2024, 299: 117086
51. Xiong Z, Lin L, Qiao S, Li L, Li Y, He S, Li Z, Liu F, Chen Y. Axial performance of seawater sea-sand concrete columns reinforced with basalt fibre-reinforced polymer bars under concentric compressive load. Journal of Building Engineering, 2022, 47: 103828
52. Nemati M, Aminian A, Rahimi S, Nematzadeh M, Jafarzadeh-Taleshi M, Thai H T. Compressive behavior of prestressed SFRCFST stub columns after heating: Effect of fresh concrete compression technique. Case Studies in Construction Materials, 2025, 23: e04968
53. Mahdi Surhan M S, Jafarzadeh H, Asadi M, Nematzadeh M. Flexural strengthening of heat-damaged RC beams with NSM CFRP strips and SFRC layer: Experimental evaluation and theoretical analysis. Journal of Building Engineering, 2025, 108: 112976
54. ACI 440.1R-15. Guide for the Design and Construction of Structural Concrete Reinforced with FRP Bars. Farmington Hills, MI: American Concrete Institute, 2015
55. CSA S806-12. Design and Construction of Buildings Components with Fiber Reinforced Polymers. Toronto: Canadian Standards Association, 2012
56. GB 50608-2020. Technical Standard for Fiber Reinforced Polymer (FRP) in Construction. Beijing: Ministry of Housing and Urban-Rural Development of the People's Republic of China, 2020
57. GB/T 50010-2010. Code for Design of Concrete Structures. Beijing: Ministry of Housing and Urban-Rural Development of the People's Republic of China, 2024
58. Xu S, Hou L, Zhang X. Shear behavior of reinforced ultra high toughness cementitious composite beams without transverse reinforcement. Journal of Materials in Civil Engineering, 2012, 24(10): 1283–1294
59. Lee D, Park S, Sim Y, Kwon O S, Lee S C. Effect of carbon nanotubes on shear behavior of PVA-ECC beams. Structures, 2025, 72: 108243
60. Gu D, Pan J, Luković M. Understanding shear-resisting mechanism in reinforced engineered cementitious composite (ECC) beams using distributed strain measurements. Engineering Structures, 2025, 327: 119612